EXAMINING THE ROLE OF K14 DEPENDENT DISULFIDE BONDING IN SKIN BARRIER HOMEOSTASIS

By:
Krystynne Aguirre Leacock

Thesis submitted to the Johns Hopkins University in conformity with the requirements for the degree of Masters of Science.

Baltimore, Maryland
May 2017

Abstract

Mammalian epidermis is a dynamic, multilayer, protective barrier that provides essential protection against environmental insults and prevents water loss. The outermost layer, the stratum corneum (SC), is composed of corneocytes, which are filled with microfibrillar keratins, surrounded by a structurally reinforced, insoluble scaffold surrounded by a lipid matrix. These components are essential for barrier function.

Previous studies in the Coulombe laboratory revealed that K14-dependent disulfide bond formation impacts the assembly, organization, and dynamics of keratin intermediate filaments in skin keratinocytes in *ex vivo* culture. In particular, cysteine (Cys or C) residue in 367 in human K14 (corresponding to Cys 373 in mouse K14) was found to play a key role in these processes. To investigate the consequences of disrupting K14-dependent disulfide bond formation for the structure and function of the epidermis we generated *Krt14*C373A mutant mice using CRISPR/Cas9 technology. Analysis of proteins isolated from adult ear and tail skin of *Krt14*C373A mice, performed under non-reducing conditions, revealed a significant decrease in disulfide-bonded K14 species of high molecular weights in comparison to wild type (WT). Additionally, the processing of filaggrin, a key effector of terminal differentiation and barrier formation, was shown to be altered alongside hyperproliferation and hyperkeratosis in the epidermis of the mutant mouse, again relative to control.

The current study continues the investigation of epidermal structure and barrier function in *Krt14*C373A mouse. At the outset of this effort we

hypothesized that thorough analysis of barrier function would reveal defects in the skin barrier of *Krt14*C373A mice relative to the control.

Here we report that adult *Krt14*C373A mice exhibit a significant increase in transepidermal water loss (TEWL) under baseline condition. Further, mutant mice show heightened sensitivity to chemical challenges at the skin barrier. Histological examinations of the adult ear uncovered a modest disruption in the SC of *Krt14*C373 mice following acetone irritation. Analysis of cornified envelope (CE) from ear and tail epidermis revealed alterations in their area and morphology. Immunofluorescence staining revealed decreases in lipid abundance in the epidermis following acetone treatment. These and other findings indicate that K14-dependent disulfide bonding is necessary for barrier homeostasis.

Advisor: Dr. Pierre Coulombe

Readers: Dr. Pierre Coulombe and Dr. Luis Garza

Acknowledgements

This thesis is based on research conducted at the Johns Hopkins Bloomberg School of Public Health from May 2016 until May 2017. This twelve-month project was completed under the supervision of Dr. Pierre Coulombe, principal investigator, and Mrs. Yajuan Guo, a Ph.D. graduate student in the Coulombe laboratory. All relevant literature was accessed through the Welch Library of the Bloomberg School of Public Health portal.

I would like to thank Dr. Pierre Coulombe for acceptance into his laboratory, his unyielding positivity, and mentorship. I would like to thank Dr. Beau Su for helping to resolve complications by crafting creative and practical solutions. I would like to extend my sincerest gratitude to Mrs. Yajuan Guo for her scientific brilliance, unyielding patience, kindness, guidance, and friendship. Additionally, I would like to thank Xia Feng and Chang-Hun Lee for creating the foundation for my project. I would also like to express my sincerest appreciation for Dr. Michelle Kerns and Mr. Andrew Nelson who spent hours helping me editing this thesis. I also would like to extend many thanks to everyone in the Coulombe laboratory, including Dr. Ryan Hobbs, Fengwrong Wang, Abigail Zieman, Justin Jacob, Brian Poll, Tara Biser, Joseph Shen, and Josh Hsu. They have all contributed to my growth and knowledge in significant ways. These interactions have made me a more prolific, perceptive, and conscientious investigator.

Outside of our laboratory, I would like to thank Dr.Luis Garza for agreeing to be my secondary reader and his insightful suggestions. Also, I would like to thank Janice Evans for her guidance and advice on science, public health, and

medicine. I would not have embarked on this journey without her. I would also like to thank Dr. Phil Jordan for his assistance with microscopy training. I would like to thank Dr. Ritankar Majumdar, a post-doctoral fellow at the National Institutes of Health, for his assistance with CE analysis.

Finally, I would like to thank my parents Dr. Darrick and Isidra Leacock and all the members of the Department of Biochemistry and Molecular Biology of the Bloomberg School of Public Health for their help and support. It is the combination of a million, minute moments of support that has enabled me to learn countless concepts and participate such an intellectually enriched and challenging environment. I will forever be grateful.

Table of Contents

Abstract ii

Acknowledgements iv

Table of Contents vi

List of Tables vii

List of Figures viii

Introduction 1
- Keratin family of proteins 1
- Layers of the epidermis 3
- K14 and Disulfide Bonding 7
- Skin barrier analysis of the *Krt14*C373A mouse model 9

Materials and Methods 14
- Animals 14
- Mouse Studies 15
- TEWL Measurements 15
- Biochemical and morphological analysis 17
- Microscopic imaging of cell and tissue preparation 20
- Quantification of images 20
- Statistical Analysis 21

Results 23
- TEWL at baseline conditions reveals a distinct phenotype in *Krt14*C373A vs. WT adult mice 23
- Histological analysis reveals alterations in *Krt14*C373A mutant mouse epidermis at baseline 25
- Acetone treatment results in increased SC fragility and morphological anomalies in *Krt14*C373A mutant epidermis 31
- K14C373A experiences hyper-activation of DAMPS 34
- Barrier disruption via acetone results in an increased TEWL *Krt14*C373A mutant mice relative to control. 36
- TEWL at baseline conditions does not reveal a distinct phenotype in *Krt14*C373A vs. WT in postnatal pups. 37
- Toluidine Blue Assay reveals no significant differences in barrier development in embryonic *Krt14*C373A mice 39

Discussion 40

Appendix 48
- Preparation of epidermal sheets by Ammonium-Thiocyanate 48
- Preparation of Cornified Envelopes 49
- Toluidine Blue Barrier Function Assay 51

References 54

Curriculum Vitae 71

List of Tables

Materials and Methods

Table 1: Table of forward and reverse sequences of mouse primers used in PCR analysis of mouse ear tissue and postnatal pup tissue.

Table 2: List of Targets and qRT-PCR Primers used.

Table 3: Genotyping PCR thermal cycler settings for both *WT* and *Krt14*C373A.

Results

Table 4: Mean TEWL and mean weight postnatal pups P0.5-P4.

Table 5: Average fold changes in DAMPs.

List of Figures

Introduction

Figure 1: The Keratin Gene Family and Structure.
Figure 2: Epidermal differentiation and layers of the epidermis
Figure 3: Overall Structure and Function of the SC within the context of the epidermis and environment
Figure 4: K14 intermediate filament structure, heterodimer, and involvement in keratinocyte differentiation.
Figure 5: The stages of CE assembly

Methods

Figure 6: Experimental Scheme of a 7-day Acetone treatment.
Figure 7: Experimental design for acetone treatment with TEWL measurement timeline

Results

Figure 8: TEWL measurements for WT and Krt14C373A adult mice.
Figure 9: Histology of untreated Krt14C373A and WT epidermis
Figure 10: Morphology of WT and Krt14C373A CE extracted from mouse tail and ear epidermis
Figure 11: Mean percentage of abnormal CEs from WT and Krt14C373A. derived from ear and tail SC
Figure 12: Quantitative analysis of CE morphology in ear and tail epidermis of WT and *Krt14*C373A
Figure 13: Histology of WT and Krt14C373A following 7-day acetone exposure.
Figure 14: Immunofluorescence-based imaging for neutral lipids in mouse ear stratum corneum
Figure 15: Fold changes in damage associated molecular patterns (DAMPs) in WT and K14C373A Mice following acetone treatment as compared to WT untreated
Figure 16: TEWL barrier recovery following acetone treatment in WT and Krt14C373A
Figure 17: Mean TEWL and Weight for postnatal pups in WT and Krt14C373A.
Figure 18: Embryonic barrier formation of WT and Krt14C373A observed via toluidine blue staining in E17.5 pups

Introduction

Keratin family of proteins

Keratin intermediate filaments play central roles in eukaryotic cells pertaining to the cytoskeletal network architecture, mechanical support, and several cellular functions in differentiated epithelium (Coulombe, 2007). In vertebrate epidermis, keratin intermediate filaments represent an astounding 85% of total proteins within a differentiated keratinocyte (Fuchs, 1995). Almost two-thirds of the keratin gene family is found in skin epithelium (Coulombe, 2007).

Within the human genome, keratin proteins originate from a group of 54 conserved keratin genes that are divided into two groups, 28 type I and 26 type II (see Figure 1a) (Schweizer et al., 2006). Type I keratin proteins are smaller and have an overall acidic charge (see Figure1a) (40- 64k; pI 4.7-7.6), whereas type II keratins as typically larger and neutral or basic in charge (50-70kDa; pI ~5.4-8.4) (Moll et al., 1982; Schweizer et al., 2006). Moreover, Type I and Type II keratin genes are regulated in a pairwise fashion *in vivo* (Kim and Coulombe, 2007). When keratin proteins polymerize they intrinsically co-assemble into coil-coiled heterodimers forming an intermediate filament network consisting of 10-12 nm wide filaments and can be visualized *in vitro* (see Figure 1b) (Steinert et al., 1976; Fuchs and Cleveland, 1998; Kim and Coulombe, 2007). Keratins possess a standard tripartite secondary structure, consisting of a central, alpha-helical rod domain flanked by 2 non-helical domains, an N-terminal head and a C-terminal tail (see Figure 1c) (Coulombe, 2007).

The expression and regulation of all keratins is context-dependent and depends on the tissue type, stage of differentiation, homeostatic state, and disease (Moll et al., 1982; O'Guin et al., 1990; Fuchs, 1995; Freedberg et al., 2001). Cell fragility, decreased adhesion, barrier dysfunction, and inflammation are hallmarks of disrupted or forfeited keratin function (Smuth et al., 2001; Lane and McLean, 2004; Segre, 2006; Arin et al., 2011, Coulombe and Lee, 2012). Keratins are involved in many diseases, likely due to their involvement in survival, death, motility, embryonic development, and cell growth (Pan et al., 2013). This thesis focuses on a specific subset of keratins, K5 and K14, a Type II and Type I intermediate filament located in the progenitor basal cells of the epidermis (Fuchs 1995).

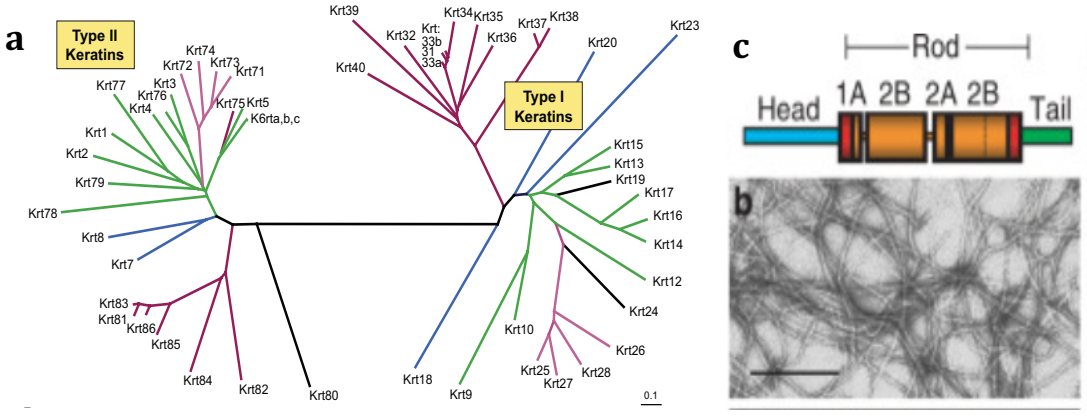

Figure 1: (a) The keratin gene family and structure. Type I and type II keratins are shown. (Adapted from Coulombe, 2001). (c) Diagram of the keratin intermediate filament structure: The configuration, of all keratins intermediate filaments, is tripartite in nature, including a head, tail, and a central α-helical rod domain (Coulombe, 2001). (b) Electron microscopy image of *in vitro* purified K5 and K14 reconstructed filaments. Scale bar = 500um. (Adapted from Gu and Coulombe, 2005).

Layers of the epidermis

Mammalian epidermis is a multilamellar arrangement of epithelial cells operating as a barrier between the inner body and the outside world. The epidermis is essential for survival; each of its layers can be recognized by unique characteristics and differences regarding permeability (Menon et al., 2012; Homalle 1853; and Dariau 1856). The epidermis is necessary for the maintenance of organismal homeostasis. It provides mechanical strength, prevents dehydration, and elicits immune responses guarding against microbes, irritants, allergens, UV radiation, pollutants, and chemical stressors.

Classically, human epidermis is described as being comprised of four distinct layers or compartments: basal layer, spinous layer, granular layer, and stratum corneum (SC). The basal layer house progenitor, mitotically-active cells and express the keratin protein partners K5 and K14. Keratinocytes in the spinous layer are post-mitotic, have initiated the process of terminal differentiation and express the keratin protein partners K1 and K10 and, at a later stage, K2 (see Figure 2) (Sadilands et al., 2009). While keratinocytes are differentiating, indeed, they move vertically in the epidermis from basal to suprabasal layers. Following a series of morphological changes, keratinocyte differentiation concludes with the formation of a condensed, enucleated, non-living corneocyte in the SC layer (Elias, 1983).

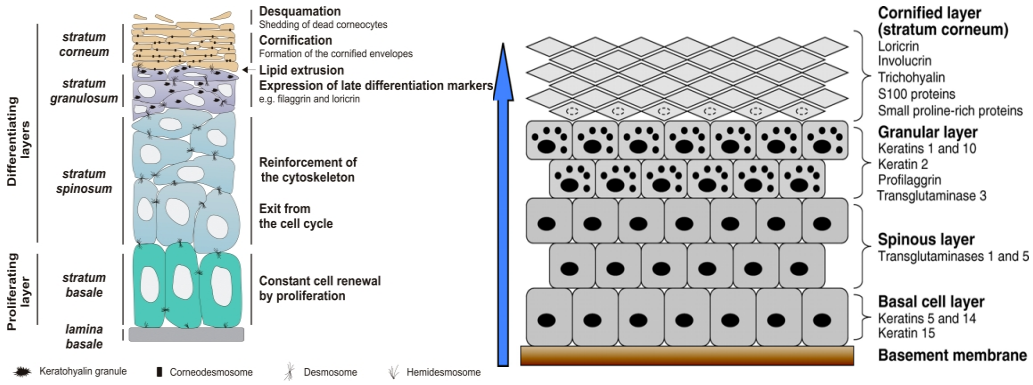

Figure 2: Epidermal differentiation and layers of the epidermis. The layers of the epidermis are a result of proliferation and differentiation beginning at the basal cell. There is a variation in expression of associated proteins. The innermost layer of the epidermis is the basal layer and proceeding outward there is the spinous, granular, and the SC (or cornified layer) (Figures are adapted from Denecke et al., 2008 and Sadilands et al., 2009).

Stratum corneum: Major determinant of barrier function of the skin

The physical barrier properties of the epidermis are mainly attributed to the SC (Blank, 1953). The SC is the outermost, terminally differentiated, non-living epidermal layer that is approximately 10-20μm and 25 cell layers thick (Smeden et al., 2014). The structure of the SC is often described as resembling a “brick in mortar,” with two principal constituents: the extracellular lipid matrix (the mortar) and the corneocytes (the bricks) (see Figure 3) (Elias, 1983).

The SC lipids make up 10% of the SC volume and the extracellular lipid matrix is a major contributor to the skin barrier. The matrix fills extracellular spaces within the SC, limits water loss, prevents electrolyte imbalance, and contains antimicrobial properties (Elias et al., 2003; Feingold, 2008). The lipid composition of the SC is comprised of approximately 50% ceramides (9 types),

25% free fatty acids, and 15% cholesterols (Feingold, 2007; Grey et al., 1982; Wetz, 2006).

Lipid precursors are contained in lamellar bodies, which are specialized organelles found in differentiated keratinocytes of the stratum granulosum layer, and are modified for SC consumption during keratinocyte differentiation (Elias and Friend, 1975). Lamellar bodies transport and in response to signals, such as increased calcium, release several substances into the SC including lipids, catabolic enzymes, IL-37, and human β-defensin 2 (Elias et al., 2014). Barrier disruption via topically-applied organic solvents (e.g., acetone) extracts lipids from the extracellular matrix and initiates a rapid homeostatic repair response resulting in expedited secretion of lamellar body products, a temporary decline in lamellar body numbers, followed by a swift assembly of new lamellar bodies (Menon et al., 1992).

In addition to the extracellular lipid matrix, the other major component of the SC are the corneocytes, which are the end products of terminal differentiation where keratins align with a key matrix protein, filaggrin, and this interaction forms dense aggregate bundles (Proksch et al., 2008). Within the corneocytes, there is a cornified envelope (CE) that is hardened, insoluble structure that is formed under the cell membrane (Denecker et. al., 2008) and serves as a support scaffold for the cell. The CE is composed of many proteins, e.g.involucrin, loricrin, trichohyalin, and small proline-rich proteins. A 5nm thick layer of lipids is covalently bonded to these proteins. The proteins are cross-linked by disulfide bonds and isopeptide bonds formed by transglutaminases below the cytoplasmic

membrane (Candi et al., 2005; Smith et al., 2006). This union of keratin and filaggrin promote the breakdown of the keratinocyte architecture and morphology, producing the corneocyte's distinctive squamous form (Proksch et al., 2008).

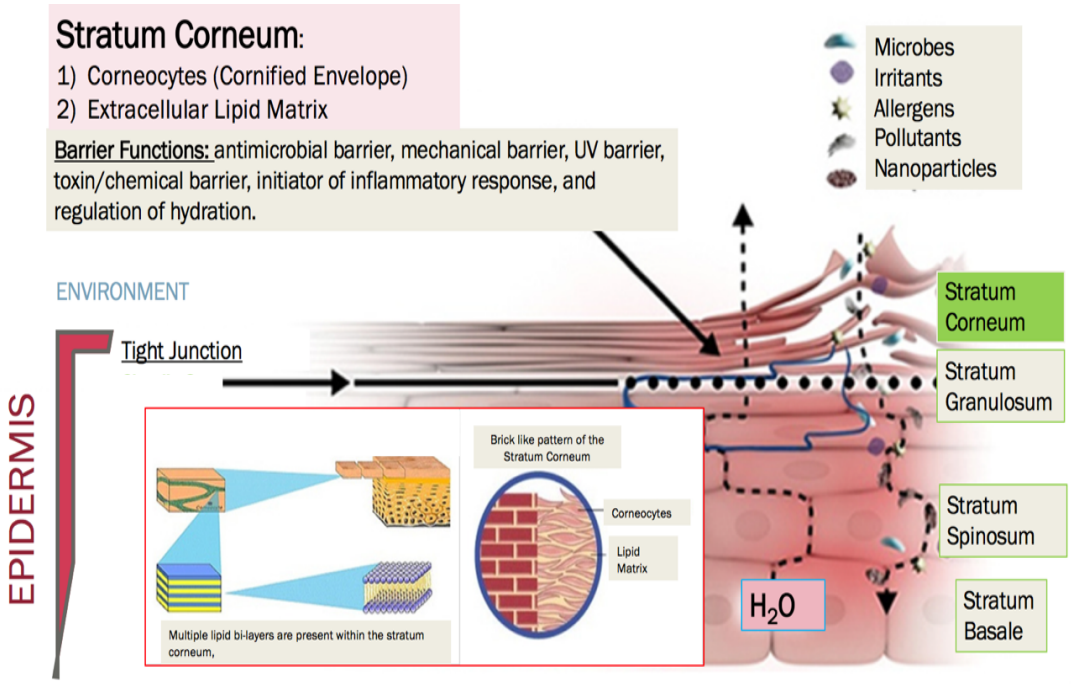

Figure 3: Overall structure and function of the SC within the context of the epidermis and environment. (These images were combined, altered & adapted from http://www.brcos.com/english/sub/sub.html?pageNum=0207).

K14 and Disulfide Bonding

During the final stages of terminal differentiation, the formation of the CE and mitochondrial lipid composition are dependent on the stabilization of keratin intermediate filaments, which is aided by intermolecular disulfide bonding (Giroud and Leblond, 1951; Kumar et al., 2015; Matolsy and Matolsy, 1970). The functionality of the SC is highly dependent on the organization of corneocytes and the extracellular lipid matrix. Ergo, keratin 14 dependent disulfide bonding is likely an essential component of assembly and organization of the SC structure and skin barrier function.

Previous studies have uncovered disulfide bonds in differentiation-specific keratins, e. g. K1 and K10, and K4 and K13 (Sun and Green, 1978; Steinert and Parry, 1993). Recently, the Coulombe laboratory reported the crystal structure of a human K14/K5 heterotypic complex (Lee et al., 2012). In the crystal lattice occurred a homotypic, trans-dimer disulfide bond involving a cysteine residue at position 367 (C367) in the central rod domain of K14 (see Figure 4b) (Lee et al., 2012). The Coulombe lab showed that this particular disulfide bond does form in skin keratinocytes in vivo, where it contributes to the formation of a perinuclear network of keratin intermediate filaments, influencing nuclear shape and size (Lee et al., 2012). Skin keratinocytes in primary culture and processed for the dual staining of K14 and disulfide-bonding uncovered their spatial coincidence in the perinuclear area following calcium-induced differentiation, (Lee et al., 2012).

Propelling the significance of keratin-dependent disulfide bonding, live cell imaging of cultured keratinocytes and the monitoring of keratin filament dynamics

revealed that, unlike wild type (WT), K14 cysteine-free variants failed to form a concentrated perinuclear IF network when expressed in a K14 null setting (Feng et al., 2015). Feng (2015) also noted enhanced nuclear movement in GFP-K14CF-expressing keratinocytes (CF, cysteine-free). However, when a single cysteine, namely C367, is reintroduced into the GFP-K14CF backbone, a significant portion of the aberrant phenotype is ameliorated (Feng 2015). This finding is significant, as there are five cysteine residues in human K14 protein located at positions: 4, 18, 40, 367, and 389 (see Figure 4a) (Lee et al., 2012). Their body of work demonstrated that K14 disulfide bonding is an important regulator of assembly, organization, and dynamics for KIFs, with emphasis on the importance of C367's contribution (see Figure 4c) (Lee et al., 2012; Feng et al., 2015). The findings of Lee and Feng have led to curiosity regarding the significance of C367 in K14 in an *in vivo* setting.

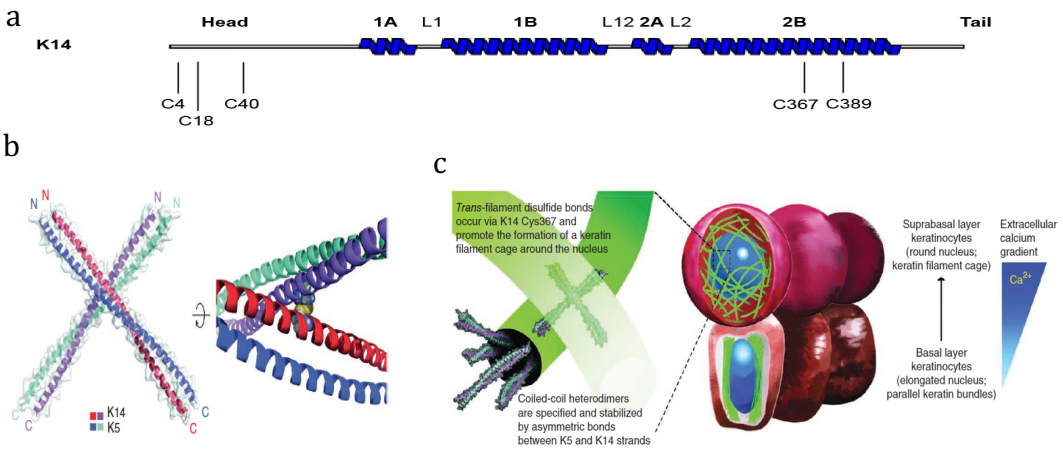

Figure 4: K14 intermediate filament structure, heterodimer, and involvement in keratinocyte differentiation. (a) The configuration, of all keratins intermediate filaments, is tripartite in nature, including a head, tail, and a central α-helical rod domain. (b)Diagram of K14/K5 heterodimer and trans-dimer disulfide bond. (c) Model of the role of keratin disulfide bonding in differentiating keratinocytes (Adapted from Lee et al., 2012).

Assembly of the SC

Normal CE assembly occurs in multiple layers of the epidermis, in three key stages: initiation, the formation of the lipid envelope, and reinforcement (see Figure 5) (Kalinin et al., 2001). Initiation of CE assembly occurs in a calcium- and differentiation-dependent manner (Kalinin et al., 2001). First, envoplakin and periplakin are expressed, generating heterotetramers, which then associate with involucrin and the plasma membrane (Kalinin et al., 2001). Afterward, the enzyme transglutaminase 1 facilitates the linkage of plakins and involucrin constructing isopeptide crosslinks that merge with desmosomal proteins (Kalinin et al., 2001). These crosslinks eventually traverse the entire, inner plasma membrane surface, while altering the properties of cell junctions and cytoskeletal interactions (Kalinin et al., 2001).

Next, the formation of the CLE occurs as the golgi complex sprouts lamellar bodies in the granular layer of the epidermis (Kalinin et al., 2001). Lamellar bodies produce specialized lipids with **ω**-hydroxy-ceramides with long fatty acid chains (cholesterol, free fatty acids, esters, and ceramides) that are delivered to the plasma membrane surface for extracellular distribution at the granular and cornified layers (Kelinin et al., 2001). These long fatty acid chains are covalently esterified by transglutaminase 1, onto scaffold proteins assembled during the initiation stage, replacing the plasma membrane, allowing interactions with the extracellular lipid matrix (Kalinin et al., 2001).

Reinforcement, the last stage, requires loricrin and small proline-rich proteins (SPRP), which constitute 80% of the cornified cell envelope (Kelinin et

al., 2008). The SPRPs and loricrin are crosslinked by transglutaminase 3 forming homodimers and heterodimers that are dispatched to the cell periphery (Kelinin et al., 2008). At the cell border, transglutaminase 1 crosslinks these proteins, fortifying the current framework. Furthermore, other proteins such as repetin, trichohyalin, cystatin, alpha, LEP/XP-5 proteins make minor contributions. (Kelinin et al., 2001). As reinforcement proceeds, other cell structures (e.g. desmosomes, microfilaments, organelles, microtubules) are destroyed. Considering intermediate filament contribution, when assembly is complete, K1, K2e, and K10 dwarf all other Ifs and are bound to residual desmoplakin, envoplakin, loricrin, involucrin, and SPRS (Kelinin et al., 2001). At the end of CE assembly, the dead corneocytes, consisting mostly of water and microfibrillar keratin, maintain flexibility and strength (Smeden et al., 2014).

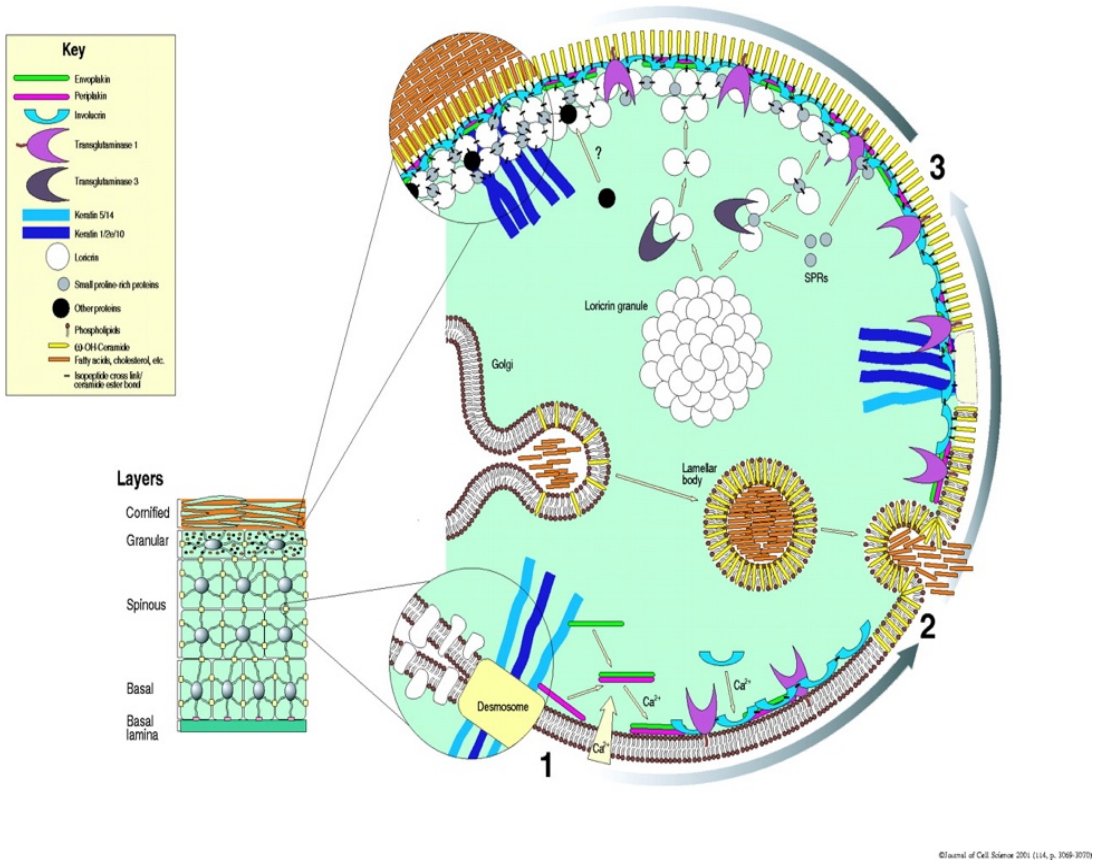

Figure 5: The stages of CE assembly. This schematic representation of CE assembly begins with (1) initiation, followed by (2) creations of CLE, and then (3) reinforcement (Kalinin et al 2001).

Skin barrier analysis of the *Krt14*C373A mouse model

The culmination of previous reports in our laboratory (by Chang-Hun Lee, Xia Feng, and Yajuan Guo) led us to hypothesize that the mutant mouse model *K14*C373A would exhibit skin barrier defects. Ultimately, Lee discovered the crystal structure of the human K5/K14 heterodimer, which includes a homotypic, trans-dimer disulfide bond at position 367 in K14. Feng revealed the importance of the C367 (orthologous to 373) on keratin network organization, assembly, and

dynamics. Yajuan Guo utilized the CRISPR/Cas9 to generate a Krt14*C373A* knock-in mice, in which the cysteine resides at position 373 was replaced with an alanine (C373A). Residue C373 in mouse K14 protein is orthologous to human C367. Guo showed that there is a decreased level of disulfide-bonded K14 species in the skin of Krt14*C373A* mice, with the overall levels of K14 remain normal. In studying these mice, Guo also found altered localization of keratinocyte differentiation markers (K14 and K10), decreased tight and adherens junction signals in immunofluorescence (ZO-1 and Claudin-3), and decreased filaggrin expression. Filaggrin and its precursor profilaggrin are key contributors to barrier homeostasis. Filaggrin overexpression or profilaggrin loss results in barrier irregularities, e.g. ichthyosis vulgaris and atopic dermatitis (eczema) in the human population disease (Proksch et al., 2008). This mouse model allows for comparative analysis of barrier structure, function, and homeostatic repair response in the postnatal and adult stages between WT and *K14C373A* mutant mice, which would enable us to elucidate the role of one disulfide bonded K14 in skin barrier function.

The present study uses a *Krt14*C373A mouse model for an initial characterization of SC structure and barrier function. In this mouse strain, the Crispr-Cas9 technology was used to replace cysteine residue 373 with an alanine (C373A) in mouse K14 (Yajuan Guo, unpublished data). The *Krt14*C373A mouse was evaluated under two conditions: 1) at baseline and 2) following topical treatment with acetone, an organic solvent known to disrupt the barrier. The central

hypothesis being tested is that barrier function is disrupted and its homeostasis perturbed in the *Krt14*C373A mouse.

We examined barrier activity at three stages: embryonic development, postnatal barrier function, and adult barrier function using a toluidine blue dye penetration assay and via measurements of trans-epidermal water loss using a Tewameter TM-300. These measures are commonly used to assess barrier function in rodents and humans since higher degrees of evaporation are associated with decreased barrier function. Skin barrier development occurs late in gestation in an established pattern, concurrent with the final stages of CE construction, which can be assessed by toluidine dye exclusion (Graubauer et al., 1989; Hardman et al., 1998).

TEWL is often used a signal for barrier recovery (Grubauer et al., 1989). Measurements of trans-epidermal water loss using a Tewameter have been validated in both humans and rodents as an accurate metric of barrier homeostasis (Fluhr et al., 2006). For example, in humans, increased in TEWL at the first 2 days of birth, and 3 months is an adequate predictor of atopic dermatitis at 1 year (Kelleher et al., 2015).

Measurements of SC permeability are not only important for water egress, but also the penetrance of pathogens, chemicals, irritants, pollutants, and allergens. To assess the SC morphology, we examined the two major components of the SC, lipid abundance and CEs. To determine barrier function in regards to immunity and barrier homeostasis, we examined cytokine transcripts of DAMPS,

which are present in the epidermis to initiate immune response in the event of a barrier breach (Chan et al., 2012).

Materials and Methods

Animals

The *Krt14*C373A mice were generated by Yajuan Guo (Coulombe laboratory) in collaboration with Dr. Vinod Ranganathan (Department of Ophthalmology) and the Johns Hopkins Transgenic Core. WT and *Krt14*C373A mice (C57BL/6 strain background) were maintained under specific pathogen-free conditions and fed rodent chow and water *ad libitum* post weaning. At 2-3 months of age mice were considered “adults”. All procedures involving mice were performed using protocols reviewed and approved by the Johns Hopkins University Animal Care and Use Committee under protocol number M016H340.

Genotyping was performed using a standard protocol and the primers listed in Table 1.

Target	Primer	Sequence (5'-->3')
Krt14	Forward	5’-AGACCAAAGGCCGTTACTG-3’
Krt14	Reverse	5’-ATTCCAGGCCCAGGTTTGAG-3’
SRY	Forward	5’-TTGTCTAGAGAGCATGGAGGGCCATGTAA-3’
SRY	Reverse	5’-CCACTCCTCTGTGACACTTTAGCCCTCCGA-3’
Krt14373A	Forward	5’-ACCAAAGGCCGTTACGC-3’
Krt14373A	Reverse	5’-TTGAGGTGGAGGAGGAGTCT-3’

Table 1: Above are the forward and reverse sequences of mouse primers used in to genotype embryonic, postnatal, and adult mice.

Mouse Studies

Topical acetone treatments of *Krt14*C373A mice

The ears of adult age-matched male WT and *Krt14*C373A mice were topically treated with 40µl of acetone twice daily for 7 days (see Figure 6). The volume of acetone was split equally between the dorsal and ventral sides of the ear. One ear was left untreated as a control. Anesthesia was administered according to IACUC standards. After treatment mice were killed and tissue was harvested for analysis.

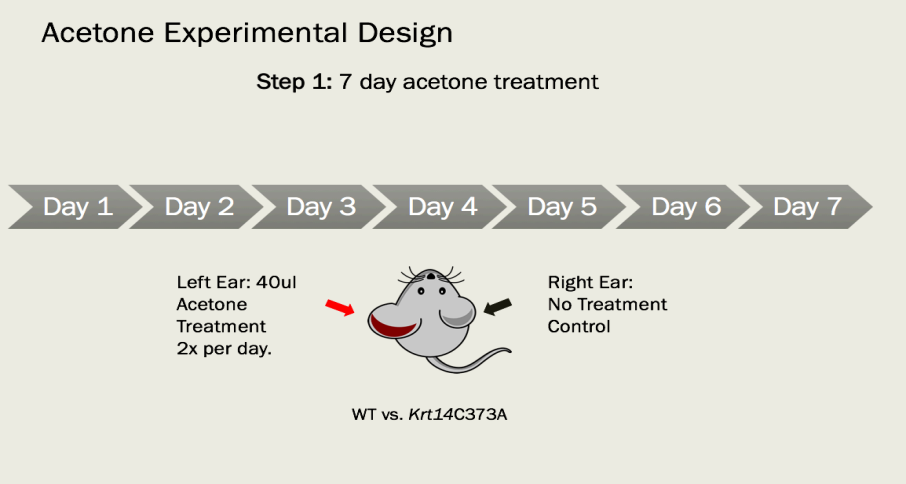

Figure 6: Experimental scheme of 7 day Acetone treatment. Male mice were treated twice per day for 7 days with 20µl of acetone on the dorsal ear and 20µl on the ventral left ear. The right ear received no treatment and was used as a control. The tissue was harvested immediately following the last acetone treatment on day 7.

TEWL Measurements

TEWL measurements were performed using a TEWAMETER TM-300 (Mecco, Warrington, PA USA) open chamber probe. The TEWL of ears of adult *Krt14*C373A and WT mice were measured at baseline and following acetone treatment regimen (treated and untreated ear) at 0, 6, 24, 48, 72, 96, and 120

hours following the last treatment of acetone (see Figure 7). During the TEWL measurements adult mice were anesthetized. Measurements were taken on the dorsal ear only. The probe was warmed for approximately 2 minutes between each measurement. The mouse was placed on its side on a napkin and the ear was flattened using toothless forceps with light pressure. The TEWL was held in place for a minimum of 30 measurements and until the alpha level was below 0.2. Since it is an open chamber device, the appropriate location of the ear was verified visually.

The TEWL of untreated dorsal lower back of postnatal pups (P0.5-P4) of *Krt14*C373A and WT mice were measured. The dorsal lower back (just above the tail) was chosen because the ear is inaccessible at these ages. TEWL measurements were performed while the pups were conscious. Measurements are sensitive to movement; therefore, pups were allowed to acclimate for 5 minutes.

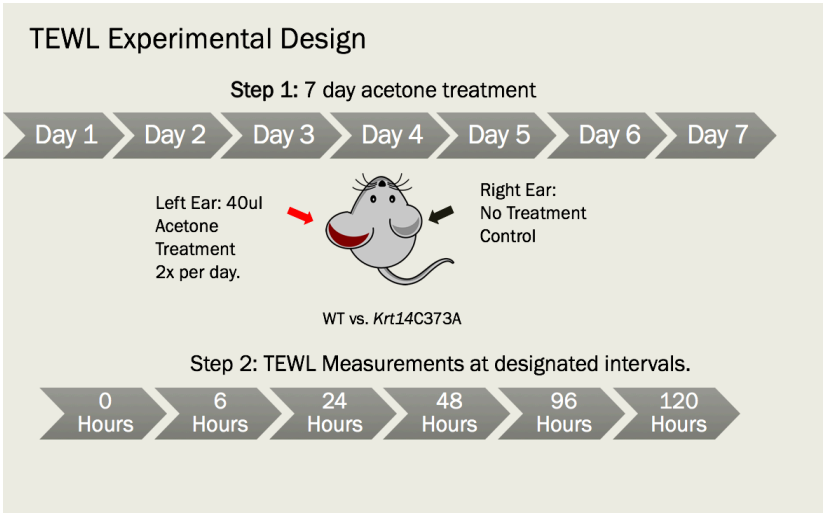

Figure 7: Experimental design for acetone treatment with TEWL measurement timeline. This experiment followed the original acetone design using adult male mice, age 2-3 months, However, this protocol includes an additional step, TEWL measurements at the above time intervals.

Toluidine blue dye skin permeability assay

A standard toluidine barrier function assay was performed on E16.5 and E17.5 WT and *Krt14*C373A following a standard protocol (DiTomasso and Foijer, 2014; Hardman et al., 1998.). Briefly, mouse embryos were dehydrated at 4°C in water-based baths with ascending then descending methanol concentrations of 2 min: 25%, 50%, 75%, 100%, 75%, 50%, 25%, 0%. The embryos were then washed in PBS (pH7.4) and stained with 0.1% toluidine blue for 1-2 minutes on ice. Pups were then washed 4 times in 50mL tubes of PBS (pH 7.4) to destain the embryos. We verified the genotype and sex of each pup.

Biochemical and morphological analysis

RNA Isolation and quantitative RT-PCR

RNA was isolated from ear tissue of adult *Krt14*C373A and WT mice treated with acetone or untreated using trizol reagent (Life Technologies). After clean up (RNAeasy Minikit, Macherey-Nagel), concentrations of RNA samples were verified via spectrophotometry and 1 μg of total RNA from each sample was reverse-transcribed (RT^2iScript, Bio-Rad). Quantitative RT-PCR was performed as described (Hobbs et al., 2015). Primer sequences are listed in Table 2.

Target	Primer Sequence
S100A1	3'- AATGTGTTCCATGCCCATTCG-5' 3'-ACCAGCACAACATACTCCTTG-5'
S100A2	3'-GAACAACCTCGATAAGGACAGTG-5' 3'-CCAGATAGCAGAATCCACCAGA-5'
S100A7A	3'-AGGAGTTGAAAGCTCTGCTCT-5' 3'-GCTCTGTGATGTAGTATGGCTG-5'
S100A8	3'-AAATCACCATGCCCTCTACAAG-5' 3'-CCCACTTTTATCACCATCGCAA-5'
S100A9	3'-ATACTCTAGGAAGGAAGGACACC-5' 3'-TCCATGATGTCATTTATGAGGGC-5'
S100A10	3'-TGGAAACCATGATGCTTACGTT-5' 3'-GAAGCCCACTTTGCCATCTC-5'
IL-1	3'-CGAAGACTACAGTTCTGCCATT-5' 3'-GACGTTTCAGAGGTTCTCAGAG-5'
IL-1ß	3'-GAAATGCCACCTTTTGACAGTG-5' 3'-TGGATGCTCTCATCAGGACA-5'
HMGB1	3'-GGCGAGCATCCTGGCTTATC-5' 3'-GGCTGCTTGTCATCTGCTG-5'
DefB3	3'-CATCTGCCTCCTTTCCTCAA-5' 3'-CTTTGCATTTCTCCTGGTGC-5'
TSLP	3'-ACGGATGGGGCTAACTTACAA-5' 3'-AGTCCTCGATTTGCTCGAACT-5'
Hspb1	3'-GGTTGCCCGATGAGTGGTC-5' 3'-CTGAGCTGTCGGTTGAGCG-5'
Hspa8	3'-CTACGCCCGATCAGACGTTT 3'-TCTCGGCACCACCTACTCC
Sprr2d	3'-GTGGGCACACAGGTGGAG 3'-GCCGAGACTACTTTGGAGAAC
Sprr3	Forward: CAGGAACCACGGTACGATCT Reverse: TTCCTGGACCATGCTCTACC
Actin	3'-TGGAATCCTGTGGCATCCATGAAAC 3'-TAAAACGCAGCTCAGTAACAGTCCG

Table 2: List of Targets and qRT-PCR Primers used.

Histology and Lipidtox immunofluorescence staining

For routine histology, ear tissue of adult *Krt14*C373A and WT mice treated with acetone or untreated were fixed in formal saline and embedded in paraffin. Sections (5µm) were fixed overnight stained with hematoxylin and eosin by JHU pathology core services following standard protocols.

For immunofluorescence Lipidtox staining a standard protocol was used (Fasta et al., 2011). Ear tissue of adult *Krt14*C373A and WT mice treated with acetone or untreated were embedded in OCT (VWR, Radnor, PA) and frozen using dry ice then sectioned at 15μm then thawed at RT 30 min following removal from a -20°C freezer. Tissue was fixed in 10% fresh formalin (diluted from 37% formaldehyde) for 10 minutes. Light was avoided during fixation step. Tissue was then washed with PBS three times. HSC Lipidtox- red neutral lipid (Invitrogen by Thermo Fisher Scientific) was diluted in PBS 1:200 and applied to the specimens. The tissue was incubated for 30 min at RT. The specimens were washed once in PBS for five minutes. DAPI was diluted 1:5000 in PBS and applied to specimens, which were then incubated for ten minutes at RT followed by three additional washes with PBS for 5 minutes each. Each slide was mounted using FluorSave.

Isolation, extraction, and preparation of cornified envelopes (CEs)

CEs were isolated from dorsal ear tissue and tail tissue from age-matched male WT and *Krt14*C373A mice. To separate dorsal from ventral ear tissue, we followed the Murine Skin Tissue Transplant protocol for ear tissue separation (the JOVE surgical video is available: https://www.jove.com/video/634/murine-skin-transplantation (removal of balbC donor skin video) (Gerod et al., 2008). Next, the epidermis was extracted using a protocol described by Roth et al. (2009) (see appendix). For extraction and preparation of CEs, a modified Wera Roth 2010 protocol (see appendix). Adult mouse ear skin or adult mouse tail skin (1cm in length) were boiled at 95° C (in place of hot water bath) for 20 min in 2ml CE

isolation buffer containing 20 mM Tris-HCl (pH 7.5), 5 mM EDTA, 10 mM dithiothreitol (DTT), and 2% sodium dodecyl sulfate (SDS). Half of the extracted sample (1ml) was flash frozen and stored for future studies. CEs were extracted from the remaining (1ml) of the CE isolate. Samples were centrifuged for 5-minutes at 5,000 × g rinsed in CE isolation buffer with 0.2% SDS, re-pelleted, re-suspended in 250 µl the washing buffer, and stored at 4°C until seeded.

For morphological evaluation, the CE isolates of dorsal ear and tail were seeded on a glass slide at a concentration of 1.5 x 10^6 CEs and 6 x 10^6 CEs, respectively, and covered. CE were isolated from at least 4 mice per genotype.

Microscopic imaging of cell and tissue preparation

For immunofluorescence staining, all images were obtained using an inverted Zeiss microscope (Thornwood, NY) fluorescence microscope with Apotome attachment and further processed using Adobe Photoshop CS2. For CE isolates, imaging and concentration calculations was completed within 48 hours of seeding and obtained using a phase contrast Zeiss microscope at 10x and 20x (Phase II) at room temperature. For toluidine blue treated embryos, images were obtained using a digital camera, a Canon RebelT5 EOS 1200D.

Quantification of images

Initial qualitative observations were made using criteria to distinguish CE as normal or abnormal. For an initial blinded assessment of CE structure, we categorized CE as abnormal if: CE size is reduced by 50%, altered aspect ratio,

and decreased phase contrast. A mean percentage of CE normal & abnormal was calculated following the examination of one hundred CE, from four individuals of the same genotype, for a total of 400 CE analyzed for each genotype (see figure 9).

A blind analysis of the CE images was completed manually using the ImageJ software and a Wacom Intuous Pro drawing pad, followed by an automated macros analysis written by Dr. Ritankar Majumdar at the NIH. A manual cell count was performed for the quantification of CE fragility. Additionally, lines were hand drawn to trace and measure the aspect ratio, circumference, and area of at least 100 CEs. Four biological replicates per genotype were examined, and 10-20 images of different regions the slides were obtained per mouse and images were further processed using Adobe Photoshop CS2. Lipidtox intensity was also measured using ImageJ (NIH).

For the toluidine blue assay, the pups were analyzed based on a 0-10 scale, where 0 represents 0% staining, and 10 represents 100% staining. These scores were averaged and compared across genotypes.

Statistical Analysis

Statistical analysis was performed using Prism Graphpad7, and a standard t-test and F-test was used to analyze CE and TEWL data. A 2-way analysis of variance (ANOVA) and individual t-tests were used to compare TEWL for the 7-day acetone barrier recovery experiment since more than 3 groups were

involved. F-tests were used to determine variance among populations. Statistical significance was confirmed if the $p<0.05$ was observed.

Results

TEWL at baseline conditions reveals a distinct phenotype in *Krt14*C373A vs. WT adult mice.

The ear skin of young adult (2-3 months old) mice homozygous for the *Krt14*C373A mutation have a statistically significant increase in baseline TEWL, by 178%, in comparison to WT controls (11.32±0.89 g/m^2/h vs. 4.07±0.44 g/m^2/h; p<0.0001) (see Figure 9). There were no statistically significant differences among WT female and male control mice (4.32 g/m^2/h±0.43 vs. 3.81±0.78 g/m^2/h; p=0.575). Female *Krt14*C373A mutant mice have a significantly greater TEWL than their mutant male constituents with a mean TEWL that is 37.8% higher (13.42 g/ m^2/h±1.11 vs. 9.75 ±1.04 g/ m^2/h where p=0.0366). Mutant females were higher than their WT female counterparts by 211% (13.42±1.11 g/ m^2/h vs. 4.32±0.433 g/m^2/h where p<0.0001). When stratified according to sex, *Krt14*C373A mutant mice exhibited significantly higher TEWL measurements than WT (Figure 8).

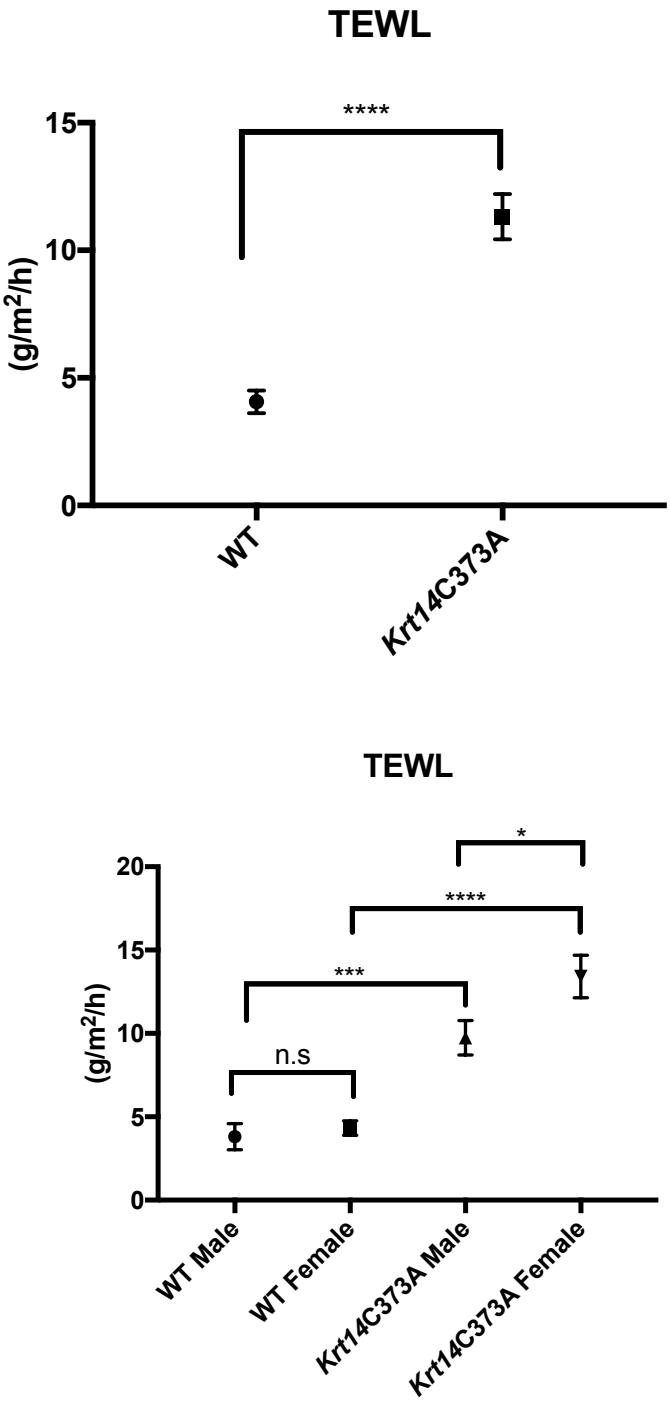

Figure 8: TEWL measurements for WT and *Krt14*C373A adult mice. TEWL measurements revealed a significant increase in TEWL for mutants in comparison to WT(above). This difference is maintained when stratified according to sex (below). *Krt14*C373A females display higher TEWL than their *Krt14*C373A male constituents. N_{WT}=24 and N_{MUT}=21 (units are in g/m^2/h). TEWL results stratified by sex (units are in g/m^2/h). Female N_{WT}=9 and N_{MUT}=12 and Male N_{WT}=12 and N_{MUT}=12.

Histological analysis reveals alterations in *Krt14*C373A mutant mouse epidermis at baseline

No macroscopic lesions could be detected in intact skin of *Krt14*C373A mice (data not shown). Tissue processing for histological examination via light microscopy revealed a modest thickening of the epidermis, along with evidence of hyperkeratosis (see Figure 9). These observations confirmed the previous findings of Yajuan Guo.

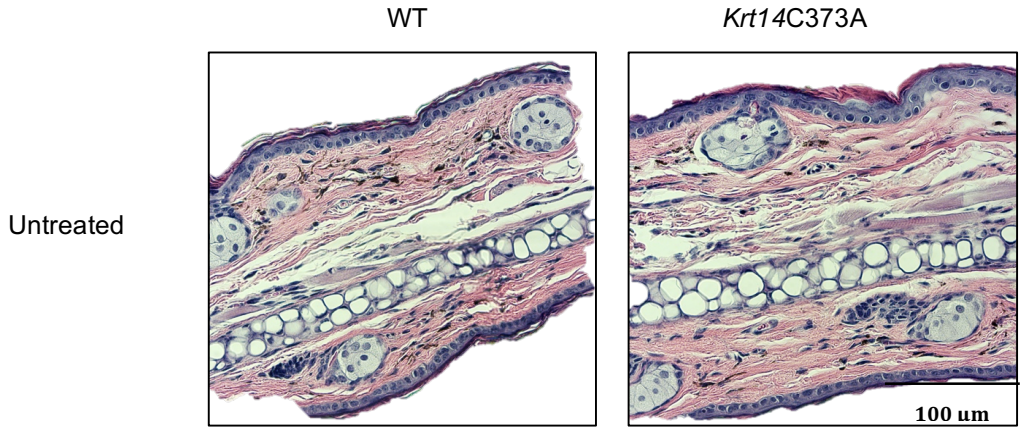

Figure 9: Histology of untreated *Krt14*C373A and WT epidermis. Histological findings indicate hyperproliferation and hyperkeratosis are present in the *Krt14*C373A SC and basal layers (N=3). Bar, 100 μm.

*Krt14*C373A mutation causes abnormal CE morphology

Analysis of CEs obtained from mice carrying the *Krt14*C373A mutation and WT controls was carried out using phase contrast microscopy. WT CE were mostly oval in shape with smooth outlines. Additionally, the WT CEs appeared relatively uniform in size and shape. By contrast, CEs harvested from *Krt14*C373A skin appeared jagged, less oval-shaped, with irregular, undulating borders (see Figure 10).

Qualitative and quantitative analyses were performed in a blinded fashion on images of CEs obtained from K14C373A and WT ear and tail skin. This revealed significant departures from WT CE morphology in mutant skin (see Figure 11 and 12). Quantitative analyses of CE images using ImageJ software confirmed these findings. Approximately 100 measurements of CEs were taken from the images obtained for four WT and four mutant mice.

Overall, qualitative analysis (normal appearing vs. abnormal appearing) revealed a higher mean percentage of abnormal CEs in dorsal ear epidermis from *Krt14*C373A mutant mice relative to controls (44.0% ± 3.16 vs. 16.5% ± 2.95; p=0.0007). Furthermore, the tail epidermis *Krt14*C373A mutant mice also had a higher percentage of abnormal CEs (55.5% ± 3.6 vs. 31.25% ± 2.17; p=0.0006), as shown in Figure 11. Quantitative analysis revealed an increased aspect ratio, lower contrast, decreased circumference, and decreased surface area or size for the mutant CEs (see Figure 12).

CEs from tail skin of *Krt14*C373A and WT mice exhibited differences that were similar to detected in ear skin. The mean aspect ratio of mutant CEs was

increased by 11% relative to WT (1.39±0.02 vs. 1.25±0.01; p<0.0001). F-test revealed variance of tail aspect ratio between populations was significant (F=2.652 and p<0.0001). The mean circumference of mutant CE was decreased by 8% relative to WT (132.5.0±1.037 μm vs. 142.9±1.042 μm p<0.0001). Finally, the mean area of mutant CEs was smaller by 8% relative to WT control (32.58±0.279 μm^2 vs. 35.4±0.269 μm^2; p<0.0001; see Figure 12). Variance between populations were not statistically significant regarding tail area or circumference (F= 1.017 and 1.118; p=0.2526 and p=0.8610).

The CE from ear tissue displayed similar differences. The CE mean aspect ratio of *Krt14*C373A mutant mice was increased by 32% and was considered to be statistically significant relative to WT, (1.317± 0.01671 vs. 1.213±0.01054; p<0.0001). F-test revealed variance of ear aspect ratio between populations was significant (F= 2.447 and p<0.0001.) The differences measured in mean surface area of *Krt14*C373A mutant were not statistically significant (29.22 ±0.42159 μm^2 vs. 29.25±0.1796 μm^2) (p = 0.9237). Mean CE circumference was smaller for mutant mouse relative to WT, by 4% (117.6±0.8704 μm vs. 122.3±0.6341 μm where p<0.0001; see Figure 12). Variance between populations was also statistically significant regarding area and circumference (F=1.412 and 1.848 where p=0.0005 and p<0.0001).

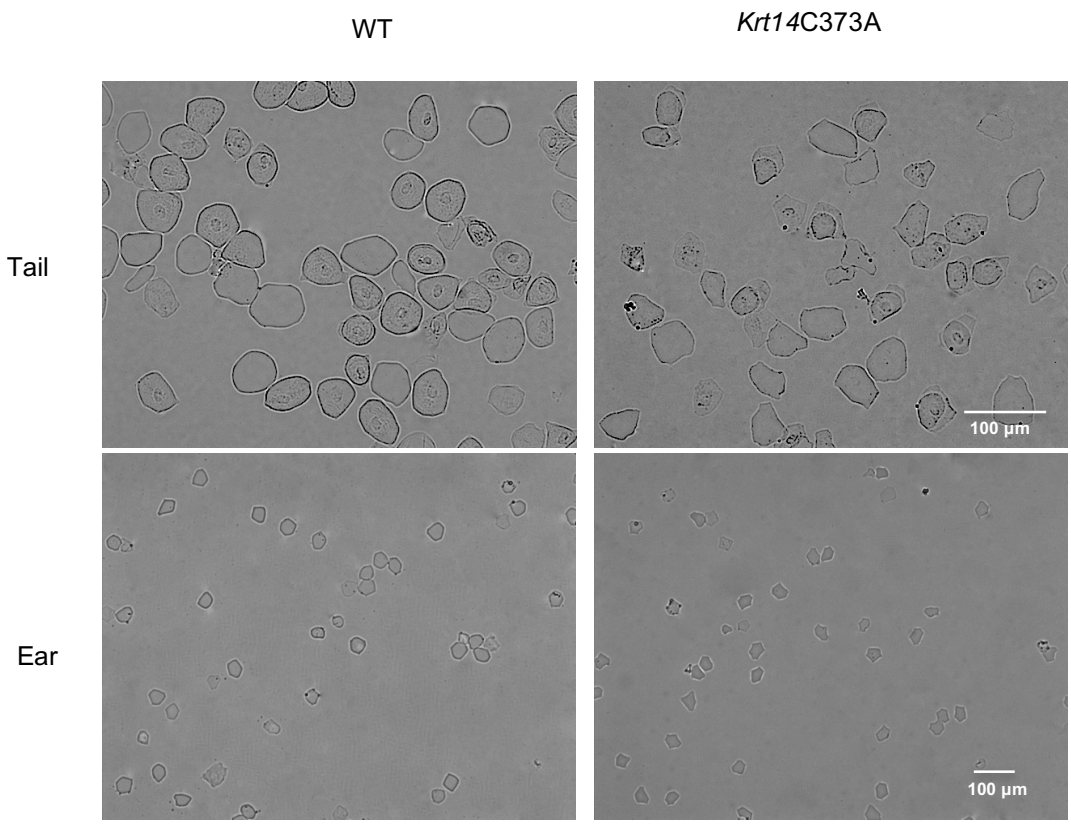

Figure 10: Morphology of WT and *Krt14*C373A CE extracted from mouse tail and ear epidermis. The top row shows CE from tail epidermis of WT and mutant adult male tissue at approximately 3 months of age (20x magnification). The bottom row shows CE from ear epidermis of WT and *Krt14*C373A adult male tissue at approximately 3 months of age (10x magnification). Mutant CEs appear to have abnormal morphology regarding size and shape. *Krt14*C373A mutant CEs appear jagged, less oval-shaped, with irregular, undulating borders (N=4). Bar, 100µm.

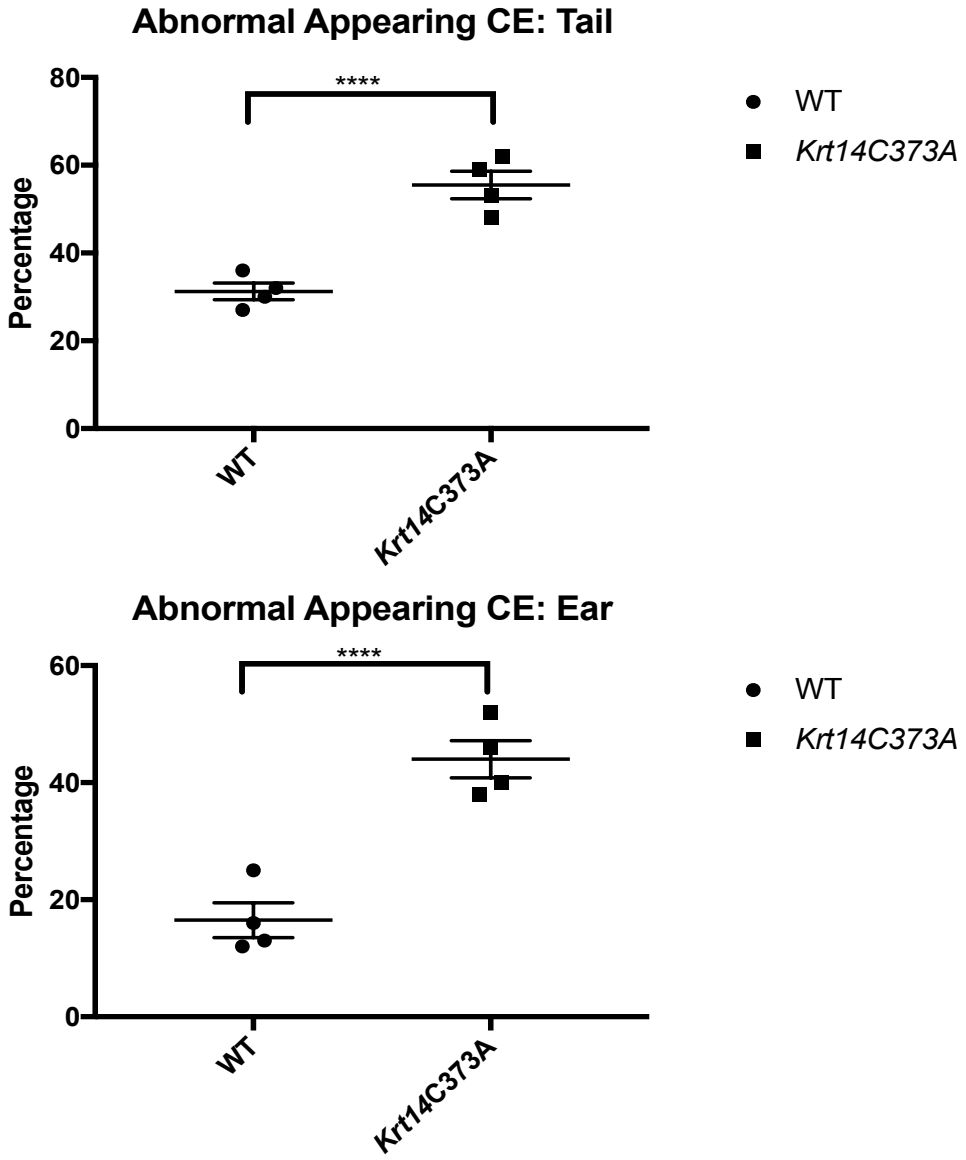

Figure 11: Mean percentage of abnormal CEs from WT and *Krt14*C373A. derived from ear and tail SC. Mutant CE has a significant increase in the mean percentage of CE that appear to be abnormal (N=4, 100 CEs were examined per individual). Error bars represent SEM.

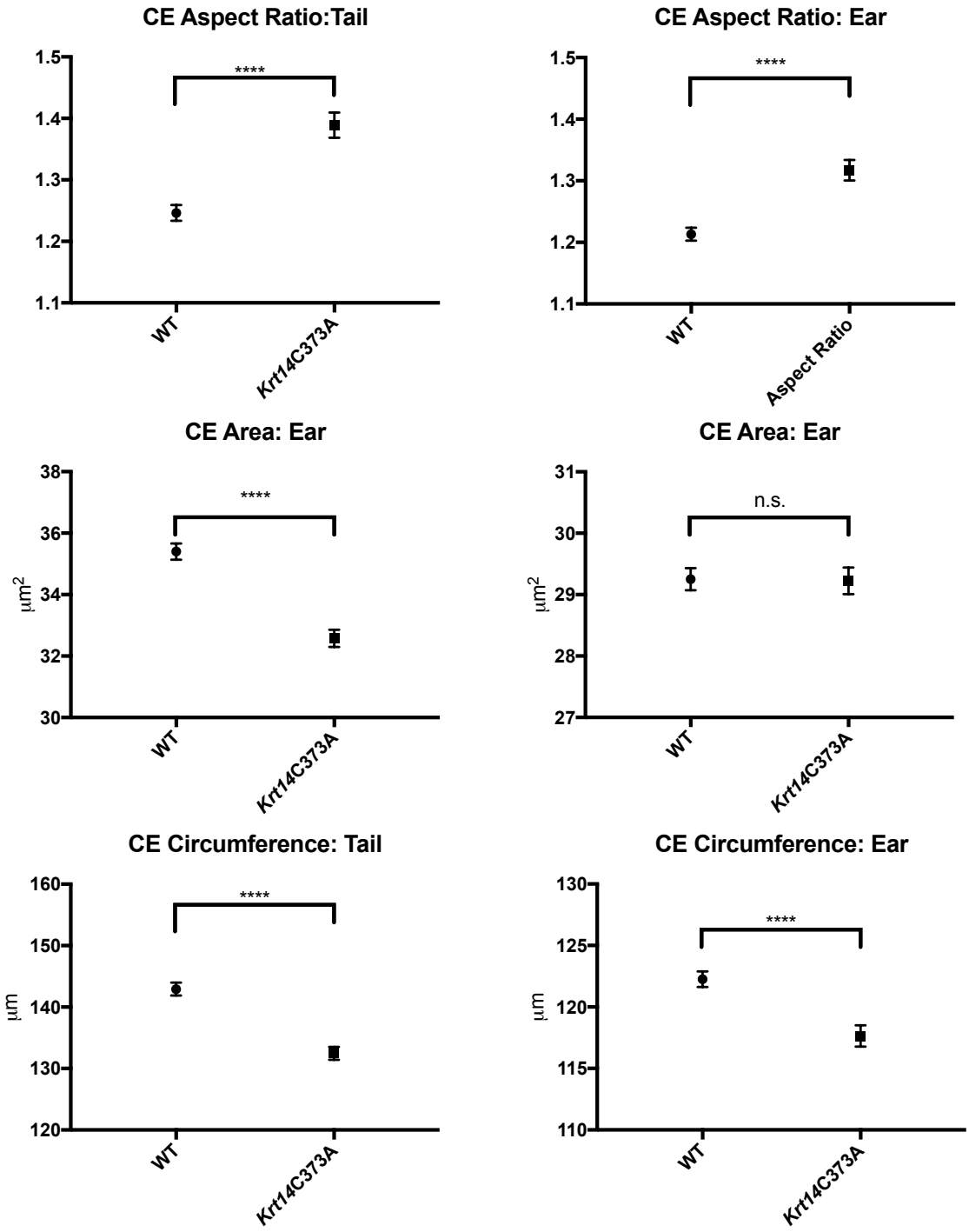

Figure 12: Quantitative Analysis of CE Morphology in Ear and Tail epidermis to display mean differences. Left column displays CE morphological analyses. *Krt14*C373A Tail CEs have an increased mean aspect ratio, decreased mean circumference, and decreased mean area relative to WT. Right column displays CE morphological analyses. Mutant Ear CE has increased aspect ratio, decreased circumference and an area that is similar when compared to the WT. Error bars represent SEM. Asterisks denote statistical significance. (N=4, 100CEs were measured per individual).

Acetone treatment results in increased SC fragility and morphological anomalies in *Krt14*C373A mutant epidermis

Histological analysis following a 7-day course of topical acetone-mediated barrier disruption resulted in mildly increased thickness of the living layers of the epidermis in WT mouse ear skin (N=3). Acetone treatment resulted in substantial disruption of the SC in *Krt14C373A* mutant ear skin, but not WT (see Figure 14). Compared with untreated *Krt14C373A* mutant ear skin (see Figure 10), the epidermis of treated *Krt14C373A* mutant ear skin appears thinner.

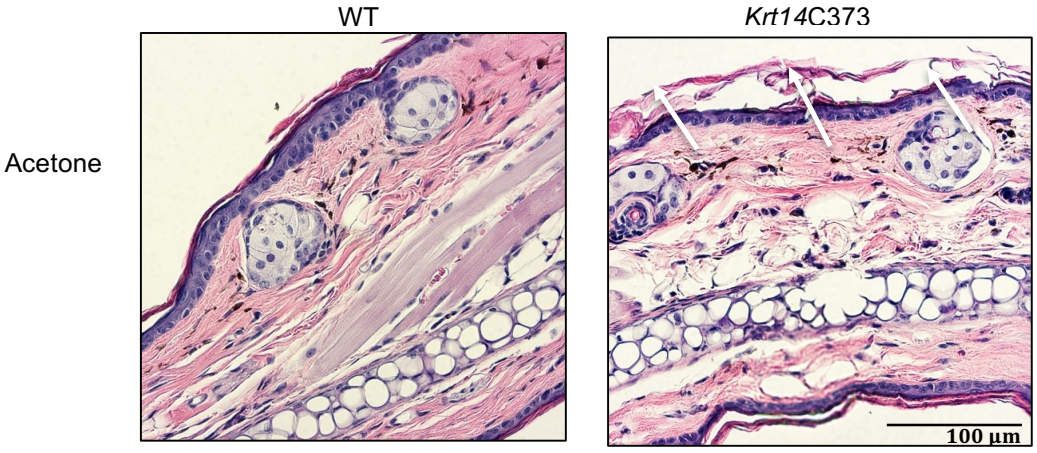

Figure 13: Histology of WT and *Krt14*C373A following 7-day acetone exposure. Findings indicate that the mutant epidermis is more fragile than WT. SC disruption is indicated by arrows. Bar, 100µm.

***Krt14*C373A mutations result in lipid loss within the SC.**

Immunofluorescence (IF) examination revealed a similar distribution of lipids in mutant and WT ear skin at baseline (N=2). After a 7-day course of acetone treatment to both side of the ears skin, however, the Lipidtox signal was decreased in the SC layers of mutant relative to WT skin (see Figure 14). The average signal intensity for WT and *Krt14*C373A lipid staining without treatment was found to be 31.98 and 26.84 on average. Therefore, at baseline mutants experiences a % decrease in lipid abundance relative to WT.

Following the application of acetone, the relative signal intensities decrease for both genotypes, with WT at 14.24 and *Krt14*C373A at 7.96. However, mutant mice experienced a 44% decrease in immunofluorescence signal following acetone treatment in comparison to WT following acetone treatment. Statistical significance was not calculated for this assay due to low number of observations. (N=2, 3 images were obtained and averaged for each genotype).

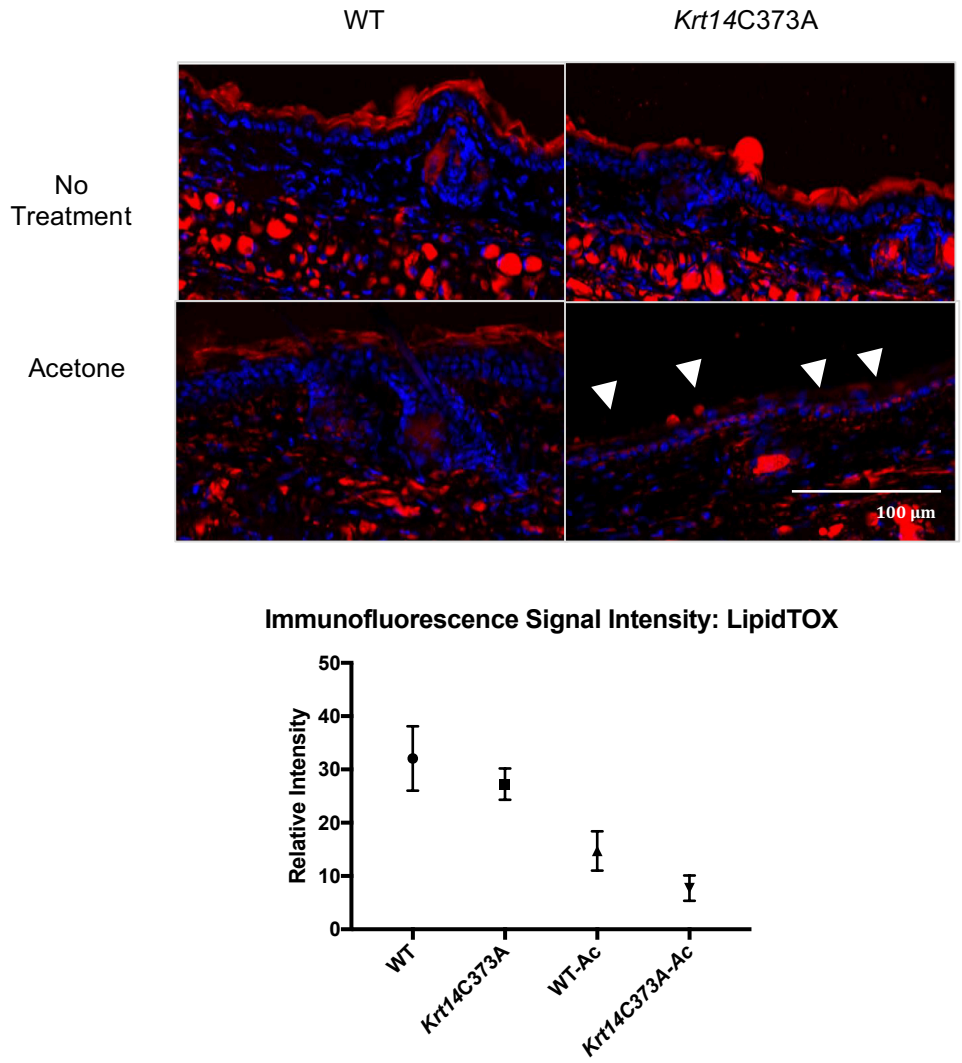

Figure 14: Immunofluorescence-based imaging for neutral lipids in mouse ear stratum corneum. LipidTOX signal intensity (red) reveals differences following treatment in WT and *Krt14*C373A following acetone treatment**.** Arrow depict areas of stratum corneum lipid loss within the Krt14373A mutant mouse. Bar,100 µm.

K14C373A experiences hyper-activation of DAMPS

Mutant transcript levels of DAMPs are elevated following acetone treatment. The mRNA levels for DAMP-encoding genes were significantly elevated for several DAMPs: S100A1, S100A2, S100A7, S100A8, S100A10, IL1-β, HMGB1, and DEFB3. The level of S100A8, S100A9, S100A10, IL-1 β, and HMCB1 experienced impressive increases of transcript levels with an average greater than 14-fold transcript level change (see Figure 15 and Table 5).

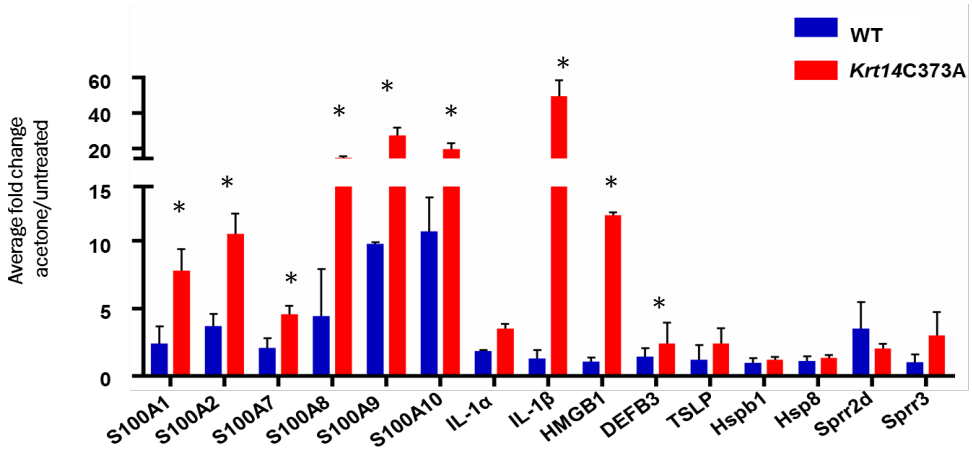

Figure 15: Fold changes in damage associated molecular patterns (DAMPs) in WT and K14C373A Mice following acetone treatment as compared to WT untreated. Asterisks represent statistically significant changes.

	WT	Krt14C373A	t-test p-value
S100A1	2.4	7.8	0.00769*
S100A2	3.7	10.5	0.00079*
S100A7	2.1	4.6	0.014786*
S100A8	4.46	14.6	0.013198*
S100A9	9.8	27.33	0.007421*
S100A10	10.7	19.6	0.000564*
IL1 A	1.87	3.5	0.083547
IL1- β	1.3	49.6	0.002986*
HMGB1	1.1	11.9	0.006162*
DEFB3	1.43	2.4	0.037618*
TSLP	1.23	2.4	0.264882
HSP b1	1	1.23	0.503762
HSP8	1.13	1.36	0.413679
Sprr 2d	1.133.5	2.03	0.424959
Sprr 3	1.04	3.03	0.243759

Table 5: Transcript level changes in found in DAMPS. Statistical significance is indicated by asterisks.

Barrier disruption via acetone results in an increased TEWL *Krt14*C373A mutant mice relative to control.

The homeostatic barrier repair response, in WT mice vs. *Krt14*C373A) was elevated and statistically significant for the first four measured time points (t-test values: P_1=0.001, P_2=0.009, P_3=0.03, P_4=0.004). WT controls treated with acetone for 7 days (twice per day) have a higher increase in TEWL that returns to baseline TEWL within approximately 72 hours. *Krt14*C373A mutant mice have an attenuated barrier response which returns to mutant baseline at approximately 120 hours following acetone treatment, which is expected considering the heightened TEWL seen at 0 hours (see figure 16).

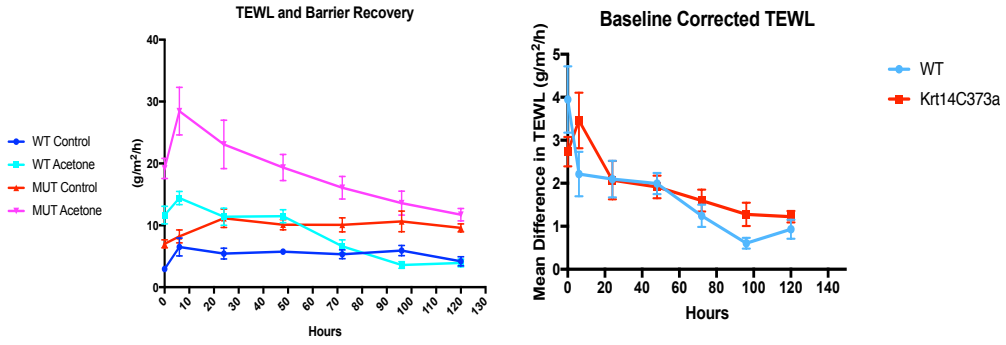

Figure 16: TEWL barrier recovery following acetone treatment in WT and *Krt14*C373A (Left) TEWL values of acetone treated ear *Krt14*C373A versus WT revealed significant increases in TEWL following acetone treatment in the *Krt14*C373A mutants suggesting increased sensitivity 120 hours after barrier disruption when compared to the WT. A 2-way ANOVA was performed and the differences were found to be statistically significant, p<0.0001. (Right) Mean difference in TEWL measurements were calculated as follows [mutant acetone treatment- mutant control] vs [WT acetone treatment- WT control] (N=6).

TEWL at baseline conditions does not reveal a distinct phenotype in *Krt14*C373A vs. WT in postnatal pups.

TEWL and weight was measured for WT and mutant postnatal pups at after birth at postnatal 0.5, 1, and 4 days. These analyses revealed no statistically significant differences between WT and mutant mice (see Figure 17). Additionally, no difference was seen when stratifying the pups according to sex (data not shown).

Age	WT TEWL ($g/m^2/h$)	WT Weight (g)	*Krt14*C373A TEWL ($g/m^2/h$)	*Krt14*C373A Weight (g)
P0.5	19.56±2.51	1.34±0.05	20.138±2.47	1.34±0.04
P1	15.87±2.16	1.44±0.03	11.94 ±5.24	1.48±0.06
P4	5.88±0.73	2.58±0.10	5.82±0.102	2.71±0.06

Table 4: Mean TEWL and mean weight for postnatal pups P0.5-P4 in WT and *Krt14*C373A. No statistically significant differences were uncovered.

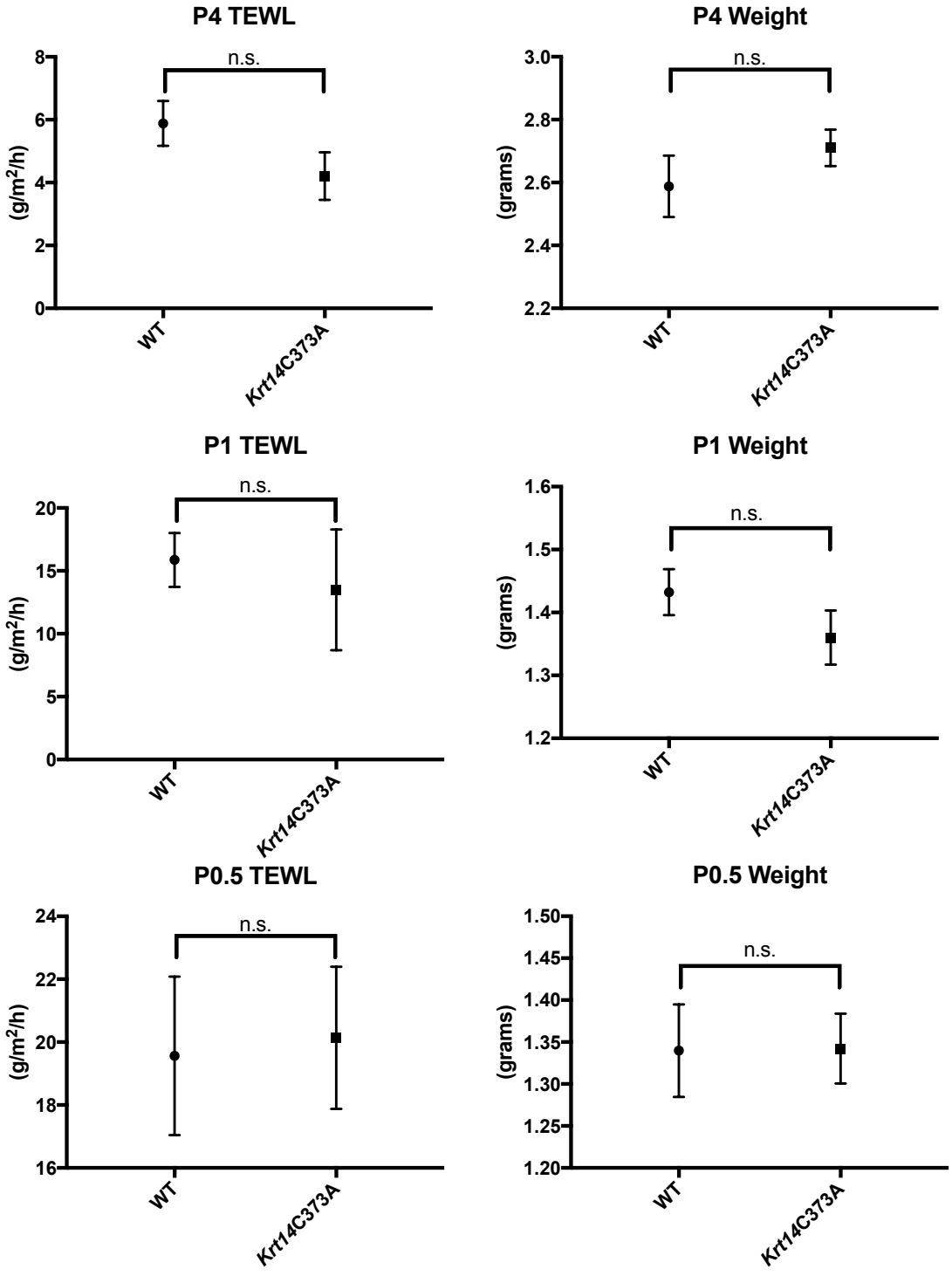

Figure 17: Mean TEWL and Weight for postnatal pups in WT and *Krt14*C373A. Row 1 shows P0.5. Row 2 shows P1. Row 3 shows P4. No statistically significant differences were found among groups observed concerning weight and TEWL. For P0.5 N_{WT}=11, N_{HET}=12, N_{MUT}=27. For P=1 the N_{WT}=10, N_{HET}=15, N_{MUT}=5. For P=4 the N_{WT}=10, N_{HET}=6, N_{MUT}=14.

Toluidine Blue Assay reveals no significant differences in barrier development in embryonic *Krt14*C373A mice

A toluidine blue dye exclusion assay was used to assess the barrier status in late stage mouse embryos (E17.5) since epidermis matures by E16.5 and development of the barrier occurs during this stage of development. Due to the sensitivity of this assay, coupled with the rapid time course of maturation of the skin barrier at approximately E16.5 during mouse development in utero, pups within the same litter were selected for comparison. We were unable to determine conclusively if the K14C373A mutation has any impact on skin barrier development from the study of 6 independent litters (see Figure 18).

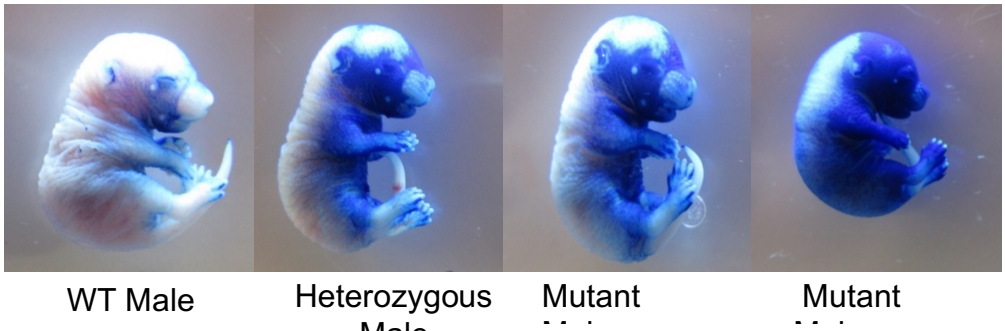

E17.5 Litter (N-6)		
Genotype	Mean Score	(N)
MUT	5.167	N=3
HET	5.50	N=1
WT	5.25	N=2

Figure 18: Embryonic barrier formation of WT and Krt14C373A observed via toluidine blue staining in E17.5 pups. One observed staining pattern displayed by an ~E17.5 litter stained with toluidine and scoring is displayed above. No obvious patterns in embryonic barrier formation was determined.

Discussion

It is widely accepted that changes in keratins, CE structure, and lipid composition, cause barrier function impairment (Ruether et al., 2006). Although K14 is primarily expressed in the basal layer, it is a long-lived protein that is present in multiple layers of the epidermis (Lizuka, 1994; Noval and Nickerson 1958; Weinstein and Scott, 1965). Studies of epithelial cell lines with RNAi-mediated K14 knockdown support the notion that K14/K5 act as negative regulators of cell differentiation (Alam et al.,2010). Keratin disulfide bonds are major contributors to the resistance of enzymatic disassembly due to its role in stereochemical configuration stabilization (Alexander and Hudson, 1954). Thus, it is conceivable that alterations in K14-dependent disulfide bonding may modulate the terminal differentiation of keratinocytes and subsequently barrier function.

This study was completed to elucidate the role of K14-dependent disulfide bonding in skin barrier function *in vivo*, using the *Krt14*C373A mouse model created by Yajuan Guo. In this mouse K14-dependent disulfide boding is reduced and altered in skin tissue, as shown by biochemical analyses, owing to the replacement of cysteine residue 373 by alanine in K14. Moreover, abnormalities were identified in several key elements as part of the barrier dysfunction phenotype in *Krt14*C373A, e.g. increased epidermal proliferation, disturbed differentiation, and anomalies involving involucrin, loricrin, and filaggrin, three key CE constituents which influence barrier function.

We hypothesized that K14-dependent disulfide-bonding is important for maintaining barrier homeostasis and challenged the *Krt14*C373A mice with an

environmental stressor that induces a skin barrier breach. Consistent with previous findings, there is a positive correlation between barrier function and disulfide bonding. Through comparisons involving TEWL, CE morphology, lipid abundance, and cytokine expression profiles between *Krt14*C373A and WT controls, we established that the modification of a single amino acid at position 373 affects skin barrier homeostasis. An elevated response in TEWL and decreased lipid abundance was noted in our mutant mice when chemically challenged with acetone in addition to enhanced protective immune response, providing evidence that strongly support our hypothesis. Taken together, these findings suggest that key morphological aspects of the barrier and the physiologic function of *Krt14*C373A mutant mouse skin are distinct from WT mice.

Even modest alterations found in individual CE, such as those found in our mutant mice, may have a cumulative effect, leading to a major consequence concerning the organization of the diffusion pathways. Potts and Francoeur (1991) established that CEs are partially responsible for lipid organization. They claim that SC permeability is 1000 times lower than values obtained for most other lipid membranes, due to the inclusion of CEs (1991). In essence, the lipid extracellular matrix allows limited fluid passage, whereas the corneocytes act as absolute barriers that must be circumnavigated. Thus, even the mild variations from a more uniform CE morphology that we observed in *Krt14*C373A may act by decreasing the tortuous nature of fluid movement through extracellular matrix of the SC, ultimately increasing the rate of evaporation from the epidermis.

In addition to CE abnormalities, mutant mouse skin features substantially reduced amount of SC lipids after barrier challenge with topical acetone and absolute lipid concentrations represent a crucial determinant of skin barrier function. Lipids contribute to the extracellular matrix and have complementary roles in addition to water regulation in the SC. Cholesterol sulfate, which is found in abundance in the SC, has a cohesive function that is relevant to desquamation (Elias et al., 1984; Williams and Elias 2014). Free fatty acids alter the pH of the SC layer, creating an acidic environment (pH 5-5.5), and pH changes can influence protease activity, and thus desquamation (Fluhr et al., 2004; Fluhr et al., 2001; Mauro, 2006). Phospholipase is a pH-sensitive enzyme and it produces glycerol which acts as a water holding agent which is significant since hydration provide signals that regulate epidermal DNA synthesis and influence inflammation (Denda et al., 1998a; Denda et al., 1998b; Scott and Harding, 1986). Lipid composition also significantly affects the skin barrier; when topical lipid mixtures are frequently applied an excess or deficiency of any individual lipid group result in an abnormal SC extracellular lipid matrix formation (Feingold, et al., 1991; Menon et al., 1992). Additionally, the lipids of the extracellular lipid matrix house proteolytic enzymes, proteolytic inhibitors, ß-defensin, cathelicidin, LL-37, and corneodesmosin (Elias, 2012). Thus, lipids are an essential component of the SC participating in both homeostasis and repair and the exaggerated lipid loss experienced by our mutant mice, within the SC, contributes to increase in trans-epidermal water loss and irregular function.

The assessment of DAMP levels following acetone treatment revealed hyperactivation in the *Krt14*C373A mice not seen in WT mice. DAMPS are recognized as a contributor to many diseases such as tumorigenesis, metastasis of cancer, autoimmune and inflammatory diseases (Chan et al., 2012). Numerous studies have uncovered that SC function is linked to the pathogenesis of multiple inflammatory skin disorders, such as atopic dermatitis, contact dermatitis, and psoriasis (Man et al., 2015). At some point in the future, the *Krt14*C373A mutant mouse strain should be assessed in terms of its susceptibility to tumorigenesis, autoimmune, or inflammatory conditions.

The physiologic assessments of TEWL also yielded interesting results. In postnatal pup epidermis revealed no significant differences in dorsal back skin of WT and *Krt14*C373A. This is consistent with the observations of Yajuan Guo, who observed no differences in disulfide bonded K14 in keratinocytes isolated from newborn back skin in WT versus *Krt14*C373A. In contrast, TEWL measurements in adult ear tissue revealed that adult *Krt14*C373A mutant mice have higher rates of TEWL in comparison to WT mice. This may be due to tissue-specific differences. For example, Quigley et al. performed an analysis of genetic architecture in adult mice examining specific cell types and signaling pathways (e.g. sonic hedgehog (Shh), Wnt, Lgr family, stem cell markers, and keratins) to monitor the effects of germline variation, skin tissue location, exogenous inflammation, or tumorigenesis (2016). Tissue locations, e.g., dorsal and tail skin, displayed significant differences among keratin gene networks and

differential cancer susceptibility, suggesting skin diseases are dependent on these conserved gene networks and their mechanisms (Quigley et al., 2016).

No obvious differences were observed in the rate of TEWL barrier recovery between WT and *Krt14*C373A when challenged with acetone. The additional time required for recovery in *Krt14*C373A is likely due to increased barrier disruption and not altered rates of barrier repair. Similarly, other studies concerning barrier recovery rate have revealed no differences in barrier rate including studies of loss of filaggrin-related to atopic dermatitis, where distinct phenotypes in barrier integrity and function are revealed when patients following tape-stripping challenges (Fischer et al., 2011). This data does not suggest any disparity in the rate of barrier repair, however more research must be completed to obtain conclusive data on barrier repair kinetics. Additionally, the TEWL findings uncovered a distinct sex difference in adult mice when the data is stratified, with higher TEWL scores belonging to the female mice.

On the subject of barrier function and sex, it has been shown that male rat fetuses develop barrier slower than females because testosterone delays development of the cutaneous barrier (Hanley et al., 1997). Conversely, estrogen supplements *in vitro* accelerate the formation of the epidermal barrier, and sex differences during barrier development *in vivo* is moderated by testosterone (Kao et al., 2001). Embryonic toluidine blue assays revealed no statistically significant differences between WT and *Krt14*C373A. Furthermore, no differences were detected in postnatal TEWL or weight.

It is likely that embryonic barrier formation and postnatal pup homeostasis is affected by k14 dependent disulfide bonding, however, the observations of embryonic and postnatal pups, were limited by several factors. Small litter sizes, coarse approximations of age, and sexually dimorphic barrier development truncated the total number of WT and *Krt14*C373A available for direct comparison within each genotype and sex. Additionally, postnatal pups were not anesthetized and TEWL readings were likely affected by heart rate and movement as TEWL measurements are not only dependent on the barrier status but also blood flow, as seen by laser doppler flowmetry (Endo et al., 2007).

Furthermore, the TEWL assessment also has limitations and results should be conservatively interpreted. TEWL evaluates the epidermal barrier in a unidirectional fashion that is formally indicative of the inside to outside barrier function (Prokschet et al., 2008). However, this not always indicative of the reverse functionality and for determination of outside-inside function other alternative assays, e.g., dye penetration and retention into the skin, need to be performed. Dye penetration assays, assessing outside to inside barrier function, are challenging to perform and interpret. It is likely there is a phenotype at earlier stages of barrier development and function however our methods may lack the sensitivity necessary for resolution under these conditions.

In the setting of EBS and Krt14 null skin, mechanical stress results in a devastating blistering response that is manifested early after birth (Coulombe, 2016). In the *Krt14*C373A mutant mice blistering does not occur in ear skin, tail, and paw tissues at any time, including early after birth. Instead, the *Krt14*C373A

mice exhibit a mild, subclinical skin phenotype under baseline conditions. Subtle changes in barrier homeostasis and physiologic response was revealed following investigation of TEWL at baseline and following provocation, with acetone. Significant alterations of SC morphology are recognized by altered CE morphology at baseline relative to WT. Collectively, these findings expand the notion that *Krt14*C373A as a contributor to terminal differentiation and barrier homeostasis in skin.

Previous findings in our lab show that the perinuclear keratin network is altered by the elimination of K14-dependent disulfide bonding, resulting in altered nucleus shape and size. Our most recent findings show the ablation of a single cysteine from K14 impacts CE structure, lipid content, and SC physiology *in vivo*. However, the molecular mechanism whereby K14-dependent disulfide bonding and, in particular, residue C373 in K14, modulate skin barrier function has yet to be defined.

Recent work in the laboratory suggests that the Hippo signaling pathway may be the mechanistic link between *Krt14*C373A and K14 disulfide bonding. Protein levels of 14-3-3 and localization of YAP in tissue samples from *Krt14*C373A differ from WT (data not shown). Additionally, our mutant mouse exhibits a defect in differentiation which was revealed by altered localization of K14, K10, and filaggrin immunofluorescence staining. One component of the Hippo pathway, YAP, has been shown inhibit terminal differentiation in mice and expand basal progenitor cells in the epidermis (Zhang, Pasolli & Fuchs, 2011). We believe we are seeing an expansion of basal progenitor cells in our mutant epidermis.

Additionally, the formation of the CE is a direct result of terminal differentiation processes; the irregular CE morphology in Krt14C373A stratum corneum may be due to underlying mechanics related to inhibited terminal differentiation.

There may be therapeutic promise in understanding the signaling pathways that relate to disulfide bonded K14 and skin barrier response and environmental stressors since barrier abnormalities are directly proportional to disease severity and such anomalies may act as a driver of disease pathogenesis (Elias, 2014). For example, researchers attribute the inflammation seen in atopic dermatitis to defects in structural and enzymatic components of the SC, with an emphasis on extracellular organization and lipid compartments (Elias, 2014).

Continued examination of the consequences of altered K14-dependent disulfide bonding *in vivo* is warranted as several common skin disorders, such as psoriasis and atopic dermatitis, involve diminished skin barrier function – yet the underlying mechanisms remain incompletely understood. Therefore, a comprehensive understanding of keratin network formation and assembly, which rely on disulfide bonded K14, in epidermal barrier function is imperative due to its potential impact on understanding a variety of common skin conditions complicated by impaired barrier function.

Appendix

Preparation of epidermal sheets by Ammonium-Thiocyanate

Wera Roth October 2009

Buffers: **1 M** Na_2HPO_4 M=141.96 g/mol 200 ml = 28.39 g

1 M NaH_2PO_4 x H_2O M=137.99g/mol 200 ml = 27.60 g

Preparation of **0.1 M** Sodium Phosphate Buffer, **pH 6.8** (see Maniatis, B.21):

250 ml 11.575 ml **1 M** Na_2HPO_4

13.425 ml **1 M** NaH_2PO_4 ad 250 ml with H_2O

Preparation of **0.5 M** Ammonium-Thiocyanate in 0.1 M Sodium Phosphate Buffer, pH 6.8:

100 ml 3.81 g Ammonium-Thiocyanate M=76.12 g/mol

ad 100 ml with 0.1 M Sodium Phosphate Buffer, pH 6.8 (prepare fresh)

1) Warm-up 0.5 M Ammonium-Thiocyanate in 0.1 M Sodium Phosphate Buffer, pH 6.8 to 37°C.
2) Prepare full-thickness skin.
3) Spread skins on plastic using forceps, epidermis up and dermis down.
4) Float skins by adding 0.5 M Ammonium-Thiocyanate solution.
5) Incubate 20-25 (max.) min at 37°C.
6) Rinse in PBS.
7) Take off epidermis.
8) Rinse in PBS. Use for subsequent applications.

Preparation of Cornified Envelopes

From: Magin Laboratory Protocol P59 by Wera Roth, 15.02.2010 (according to Hohl D. et al., 1991, J. Biol. Chem. 266: 6626-6636 and Jarnik M. et al., 1996, J. Cell Science 109: 1381-1391)

1) Preparation of epidermal sheets using NH4-Thiocyanate solution (see P58).
2) Alternatively, newborn total skin can be used.
3) Cut tissue into pieces.
4) Epidermal sheets / total skin are heated with stirring in CE-extraction buffer for
5) 20-40 min at 95°C. Use 5 ml per epidermis and 10 ml per skin on a boiling
6) water bath with vigorous stirring.
    a. Optional: Quick-freeze in LN2 and store at -80°C until further processing.
7) CEs are collected by centrifugation at 5000 x g for 15 min at RT.
8) CEs are washed twice at RT with CE-extraction buffer containing 0.2% SDS.
9) CEs are collected by centrifugation at 5000 x g for 15 min.
10) Suspend in 2% SDS solution.
11) Adjust/determine CE concentration in a hemacytometer.
12) Sonication (Branson 2210 cup sonicator) at 4°C, 20°C, 30°C, and 60°C.

13) At various time points, remove CE aliquots from the sonicator, count with the

14) hemacytometer and photograph.

    a. Final CE preps can be stored at 4°C for up to several weeks.

    b. Optional: Drop CEs (50µl) on a glass slide and embed in Mowiol.

15) CE-extraction buffer:

    a. M Tris/HCl, pH 8.5

    b. 2% SDS

    c. 20 mM DTT

    d. 5 mM EDTA

Toluidine Blue Barrier Function Assay

From DiTamasso et al., 2014 and Hardman et al., 1998

Materials and Reagents

1) E18.5 embryos from mice
2) Chilled methanol in water (25%, 50%, 75% and 100% MetOH)
3) 0.1% toluidine blue (in water) (Sigma-Aldrich)
4) Chilled 1x PBS (pH 7.4) (Sigma-Aldrich, catalog number: P4417)

   (Recipe: 1x PBS (pH 7.4) 1 tablet per 200 ml dH_2O)

Equipment

1) Forceps
2) Camera

Procedure

1) Isolate uterus from pregnant females to obtain E18.5 embryos.
2) Euthanize embryos by immersion in ice cold PBS for 30 min.
3) At 18.5 days gestation, cull mother by cervical dislocation. Make a ventral incision and remove the uterine horn containing the embryos. To euthanize embryos, immerse entire uterus containing embryos in ice cold PBS for 30 min. Separate embryos and remove from uterus. Check that embryos have been successfully euthanized by pinching toe or tail with forceps. If embryo responds, place back into ice cold PBS and check

every 5 min. Once embryos are unresponsive/culled, proceed to the next step.

4) Finger/toe clip individual embryos for identification. This is especially important when crossing heterozygous mice. The digits can be used for genotyping the embryos.

5) Passage embryos through chilled methanol gradient, taking 2 min per step. It is crucial to have all solutions at 4 degrees centigrade. Keep solutions on ice throughout protocol.

   a. 25% methanol in water
   b. 50% methanol in water
   c. 75% methanol in water
   d. 100% methanol
   e. 75% methanol in water
   f. 50% methanol in water
   g. 25% methanol in water
   h. 100% water or PBS

6) Immerse embryos in 0.1% toluidine blue solution in water for 1-2 min on ice.

7) Destain embryos in PBS (pH 7.4) until a dye pattern emerges (in case of barrier defect) or until dye is washed away (in case of intact barrier) on ice.

8) Take pictures of individual embryos and if relevant genotype embryos. See also Figure 1 for some examples of intact barriers and barrier acquisition defects.

References

Alexander, P., & Hudson, R. F. (1954). Wool-its chemistry and physics Chapman and Hall Ltd; WC.

Angelova‐Fischer, I., Mannheimer, A., Hinder, A., Ruether, A., Franke, A., Neubert, R. H., . . . Zillikens, D. (2011). Distinct barrier integrity phenotypes in filaggrin‐related atopic eczema following sequential tape stripping and lipid profiling. Experimental Dermatology, 20(4), 351-356.

Blank, I. H. (1953). Further observations on factors which influence the water content of the stratum corneum. Journal of Investigative Dermatology, 21(4), 259-271.

Brandner, J., & Proksch, E. (2006). Epidermal barrier function: Role of tight junctions. Skin Barrier.New York: Taylor and Francis, , 191-210.

Brandner, J. M., Kief, S., Grund, C., Rendl, M., Houdek, P., Kuhn, C., . . . Moll, I. (2002). Organization and formation of the tight junction system in human epidermis and cultured keratinocytes. European Journal of Cell Biology, 81(5), 253-263.

Brandner, J. M., Kief, S., Wladykowski, E., Houdek, P., & Moll, I. (2006). Tight junction proteins in the skin. Skin Pharmacology and Physiology, 19(2), 71-77. doi:91973 [pii]

Candi, E., Schmidt, R., & Melino, G. (2005). The cornified envelope: A model of cell death in the skin. Nature Reviews Molecular Cell Biology, 6(4), 328-340.

Candi, E., Tarcsa, E., Digiovanna, J. J., Compton, J. G., Elias, P. M., Marekov, L. N., & Steinert, P. M. (1998). A highly conserved lysine residue on the head domain of type II keratins is essential for the attachment of keratin intermediate filaments to the cornified cell envelope through isopeptide crosslinking by transglutaminases. Proceedings of the National Academy of Sciences of the United States of America, 95(5), 2067-2072.

Chan, J. K., Roth, J., Oppenheim, J. J., Tracey, K. J., Vogl, T., Feldmann, M., . . . Nanchahal, J. (2012). Alarmins: Awaiting a clinical response. The Journal of Clinical Investigation, 122(8), 2711-2719. doi:10.1172/JCI62423 [doi]

Coulombe, P. A., & Lee, C. (2012). Defining keratin protein function in skin epithelia: Epidermolysis bullosa simplex and its aftermath. Journal of Investigative Dermatology, 132(3), 763-775.

Denda, M., Sato, J., Masuda, Y., Tsuchiya, T., Koyama, J., Kuramoto, M., . . . Feingold, K. R. (1998). Exposure to a dry environment enhances epidermal permeability barrier function. Journal of Investigative Dermatology, 111(5), 858-863.

Denda, M., Sato, J., Tsuchiya, T., Elias, P. M., & Feingold, K. R. (1998). Low humidity stimulates epidermal DNA synthesis and amplifies the hyperproliferative response to barrier disruption: Implication for seasonal exacerbations of inflammatory dermatoses. Journal of Investigative Dermatology, 111(5), 873-878.

Denda, M., Wood, L. C., Emami, S., Calhoun, C., Brown, B. E., Elias, P. M., & Feingold, K. R. (1996). The epidermal hyperplasia associated with repeated barrier disruption by acetone treatment or tape stripping cannot be attributed to increased water loss. Archives of Dermatological Research, 288(5), 230-238.

Denecker, G., Ovaere, P., Vandenabeele, P., & Declercq, W. (2008). Caspase-14 reveals its secrets. The Journal of Cell Biology, 180(3), 451-458. doi:10.1083/jcb.200709098 [doi]

Djalilian, A. R., McGaughey, D., Patel, S., Seo, E. Y., Yang, C., Cheng, J., . . . Segre, J. A. (2006). Connexin 26 regulates epidermal barrier and wound remodeling and promotes psoriasiform response. The Journal of Clinical Investigation, 116(5), 1243-1253. doi:10.1172/JCI27186 [doi]

Duriau, F. (1856). Recherches expérimentales sur l'absorption et l'exhalation par le tégument externe, sur la température animale, la circulation, et la respiration, ou essai sur l'action physiologique des bains d'eau Rignoux.

Elias, P. M. (2005). Stratum corneum defensive functions: An integrated view. Journal of General Internal Medicine, 20(5), 183-200.

Elias, P. M. (2012). Structure and function of the stratum corneum extracellular matrix. Journal of Investigative Dermatology, 132(9), 2131-2133.

Elias, P. M. (2014). Lipid abnormalities and lipid-based repair strategies in atopic dermatitis. Biochimica Et Biophysica Acta (BBA)-Molecular and Cell Biology of Lipids, 1841(3), 323-330.

Elias, P. M., Cooper, E. R., Korc, A., & Brown, B. E. (1981). Percutaneous transport in relation to stratum corneum structure and lipid composition. Journal of Investigative Dermatology, 76(4), 297-301.

Elias, P. M., & Friend, D. S. (1975). The permeability barrier in mammalian epidermis. J Cell Biol, 65(1), 180-191.

Elias, P. M., Gruber, R., Crumrine, D., Menon, G., Williams, M. L., Wakefield, J. S., . . . Uchida, Y. (2014). Formation and functions of the corneocyte lipid envelope (CLE). Biochimica Et Biophysica Acta (BBA)-Molecular and Cell Biology of Lipids, 1841(3), 314-318.

Elias, P. M., Mcnutt, N. S., & Friend, D. S. (1977). Membrane alterations during cornification of mammalian squamous epithelia: A freeze‐fracture, tracer, and thin‐section study. The Anatomical Record, 189(4), 577-593.

Elias, P. M., & Wakefield, J. S. (2014). Mechanisms of abnormal lamellar body secretion and the dysfunctional skin barrier in patients with atopic dermatitis. Journal of Allergy and Clinical Immunology, 134(4), 781-791. e1.

Elias, P., Feingold, K., & Fluhr, J. (2003). Skin as an organ of protection. Dermatology in General Medicine.IM Friedberg, AZ Eisen, K.Wolff, KF Austen, LA Goldsmith, and SI Katz, Editors.McGraw Hill, New York, , 107-118.

Elias, P. M., Matsuyoshi, N., Wu, H., Lin, C., Wang, Z. H., Brown, B. E., & Stanley, J. R. (2001). Desmoglein isoform distribution affects stratum corneum structure and function. The Journal of Cell Biology, 153(2), 243-249.

Endo, K., Suzuki, N., Yoshida, O., Sato, H., & Fujikura, Y. (2007). The barrier component and the driving force component of transepidermal water loss and

their application to skin irritant tests. Skin Research and Technology, 13(4), 425-435.

Feingold, K. R., & Elias, P. M. (2014). Role of lipids in the formation and maintenance of the cutaneous permeability barrier. Biochimica Et Biophysica Acta (BBA)-Molecular and Cell Biology of Lipids, 1841(3), 280-294.

Feingold, K. R., Mao-Qiang, M., Proksch, E., Menon, G. K., Brown, B. E., & Elias, P. M. (1991). The lovastatin-treated rodent: A new model of barrier disruption and epidermal hyperplasia. Journal of Investigative Dermatology, 96(2), 201-209.

Feingold, K. R. (2007). Thematic review series: Skin lipids. the role of epidermal lipids in cutaneous permeability barrier homeostasis. Journal of Lipid Research, 48(12), 2531-2546. doi:R700013-JLR200 [pii]

Feng, X., & Coulombe, P. A. (2015). A role for disulfide bonding in keratin intermediate filament organization and dynamics in skin keratinocytes. The Journal of Cell Biology, 209(1), 59-72. doi:10.1083/jcb.201408079 [doi]

Festa, E., Fretz, J., Berry, R., Schmidt, B., Rodeheffer, M., Horowitz, M., & Horsley, V. (2011). Adipocyte lineage cells contribute to the skin stem cell niche to drive hair cycling. Cell, 146(5), 761-771.

Fluhr, J. W., Behne, M. J., Brown, B. E., Moskowitz, D. G., Selden, C., Mao-Qiang, M., . . . Feingold, K. R. (2004). Stratum corneum acidification in neonatal skin: Secretory phospholipase A 2 and the sodium/hydrogen antiporter-1 acidify neonatal rat stratum corneum. Journal of Investigative Dermatology, 122(2), 320-329.

Fluhr, J. W., Feingold, K. R., & Elias, P. M. (2006). Transepidermal water loss reflects permeability barrier status: Validation in human and rodent in vivo and ex vivo models. Experimental Dermatology, 15(7), 483-492.

Fluhr, J. W., Kao, J., Ahn, S. K., Feingold, K. R., Elias, P. M., & Jain, M. (2001). Generation of free fatty acids from phospholipids regulates stratum corneum acidification and integrity. Journal of Investigative Dermatology, 117(1), 44-51.

Fuchs, E. (1995). Keratins and the skin. Annual Review of Cell and Developmental Biology, 11(1), 123-154.

Fuchs, E., & Green, H. (1980). Changes in keratin gene expression during terminal differentiation of the keratinocyte. Cell, 19(4), 1033-1042.

Fuchs, E., & Weber, K. (1994). Intermediate filaments: Structure, dynamics, function and disease. Annual Review of Biochemistry, 63(1), 345-382.

Fuchs, E., & Cleveland, D. W. (1998). A structural scaffolding of intermediate filaments in health and disease. Science (New York, N.Y.), 279(5350), 514-519.

Furuse, M., Hata, M., Furuse, K., Yoshida, Y., Haratake, A., Sugitani, Y., . . . Tsukita, S. (2002). Claudin-based tight junctions are crucial for the mammalian epidermal barrier: A lesson from claudin-1-deficient mice. The Journal of Cell Biology, 156(6), 1099-1111. doi:10.1083/jcb.200110122 [doi]

Garrod, K. R., & Cahalan, M. D. (2008). Murine skin transplantation. JoVE (Journal of Visualized Experiments), (11), e634-e634.

Ghadially, R., Brown, B. E., Hanley, K., Reed, J. T., Feingold, K. R., & Elias, P. M. (1996). Decreased epidermal lipid synthesis accounts for altered barrier function in aged mice. Journal of Investigative Dermatology, 106(5), 1064-1069.

Giroud, A., & Leblond, C. (1951). The keratinization of epidermis and its derivatives, especially the hair, as shown by x‐ray diffraction and histochemical studies. Annals of the New York Academy of Sciences, 53(1), 613-626.

Gray, G., White, R., Williams, R., & YARDLEYMRC, H. (1982). Lipid composition of the superficial stratum corneum cells of pig epidermis. British Journal of Dermatology, 106(1), 59-63.

Grubauer, G., Elias, P. M., & Feingold, K. R. (1989). Transepidermal water loss: The signal for recovery of barrier structure and function. Journal of Lipid Research, 30(3), 323-333.

Hanley, K., Rassner, U., Jiang, Y., Vansomphone, D., Crumrine, D., Komuves, L., . . . Williams, M. L. (1996). Hormonal basis for the gender difference in epidermal barrier formation in the fetal rat. acceleration by estrogen and delay by testosterone. The Journal of Clinical Investigation, 97(11), 2576-2584. doi:10.1172/JCI118706 [doi]

Hardman, M. J., Sisi, P., Banbury, D. N., & Byrne, C. (1998). Patterned acquisition of skin barrier function during development. Development (Cambridge, England), 125(8), 1541-1552.

Hobbs, R. P., DePianto, D. J., Jacob, J. T., Han, M. C., Chung, B., Batazzi, A. S., . . . Ong, S. (2015). Keratin-dependent regulation of aire and gene expression in skin tumor keratinocytes. Nature Genetics, 47(8), 933-938.

Homolle, E. (1853). Experiences physiologiques sur l'absorption par le tegument externe chez l'homme dans le bain Typographie Félix Malteste et Cie.

Ishida-Yamamoto, A., & - Iizuka, H.Structural organization of cornified cell envelopes and alterations in inherited skin disorders Wiley Online Library.

Kelleher, M., Dunn-Galvin, A., Hourihane, J. O., Murray, D., Campbell, L. E., McLean, W. I., & Irvine, A. D. (2015). Skin barrier dysfunction measured by transepidermal water loss at 2 days and 2 months predates and predicts atopic dermatitis at 1 year. Journal of Allergy and Clinical Immunology, 135(4), 930-935. e1.

Krug, S. M., Schulzke, J. D., & Fromm, M. (2014). Tight junction, selective permeability, and related diseases. Seminars in Cell & Developmental Biology, , 36 166-176.

Kumar, V., Bouameur, J. E., Bar, J., Rice, R. H., Hornig-Do, H. T., Roop, D. R., . . . Magin, T. M. (2015). A keratin scaffold regulates epidermal barrier formation, mitochondrial lipid composition, and activity. The Journal of Cell Biology, 211(5), 1057-1075. doi:10.1083/jcb.201404147 [doi]

Langbein, L., Grund, C., Kuhn, C., Praetzel, S., Kartenbeck, J., Brandner, J. M., . . . Franke, W. W. (2002). Tight junctions and compositionally related junctional structures in mammalian stratified epithelia and cell cultures derived therefrom. European Journal of Cell Biology, 81(8), 419-435.

Lee, C., Kim, M., Chung, B. M., Leahy, D. J., & Coulombe, P. A. (2012). Structural basis for heteromeric assembly and perinuclear organization of keratin filaments. Nature Structural & Molecular Biology, 19(7), 707-715.

Leung, D. Y. (1999). Pathogenesis of atopic dermatitis. Journal of Allergy and Clinical Immunology, 104(3), S99-S108.

Ma, L., Yamada, S., Wirtz, D., & Coulombe, P. A. (2001). A'hot-spot'mutation alters the mechanical properties of keratin filament networks. Nature Cell Biology, 3(5), 503-506.

Maass, K., Ghanem, A., Kim, J. S., Saathoff, M., Urschel, S., Kirfel, G., . . . Willecke, K. (2004). Defective epidermal barrier in neonatal mice lacking the C-terminal region of connexin43. Molecular Biology of the Cell, 15(10), 4597-4608. doi:10.1091/mbc.E04-04-0324 [doi]

Madison, K. C. (2003). Barrier function of the skin:“la raison d'etre” of the epidermis. Journal of Investigative Dermatology, 121(2), 231-241.

Man, G., Elias, P. M., & Man, M. (2015). Therapeutic benefits of enhancing permeability barrier for atopic eczema. Dermatologica Sinica, 33(2), 84-89.

Man, Y. S., Trolove, C., Tattersall, D., Thomas, A. C., Papakonstantinopoulou, A., Patel, D., . . . O'Toole, E. A. (2007). A deafness-associated mutant human connexin 26 improves the epithelial barrier in vitro. Journal of Membrane Biology, 218(1-3), 29-37.

Matoltsy, A. G., & Matoltsy, M. N. (1970). The chemical nature of keratohyalin granules of the epidermis. The Journal of Cell Biology, 47(3), 593-603.

Mauro, T. (2006). SC pH: Measurement, origins, and functions. Skin Barrier.New York: Taylor & Francis Group, , 223-230.

McLachlan, A. d. (1978). Coiled coil formation and sequence regularities in the helical regions of α-keratin. Journal of Molecular Biology, 124(1), 297-304.

Menon, G. K., Feingold, K. R., Mao-Qiang, M., Schaude, M., & Elias, P. M. (1992). Structural basis for the barrier abnormality following inhibition of HMG CoA reductase in murine epidermis. Journal of Investigative Dermatology, 98(2), 209-219.

NOVAL, J. J., & NICKERSON, W. J. (1959). Decomposition of native keratin by streptomyces fradiae. Journal of Bacteriology, 77(3), 251-263.

Omary, M. B., Coulombe, P. A., & McLean, W. I. (2004). Intermediate filament proteins and their associated diseases. New England Journal of Medicine, 351(20), 2087-2100.

Pan, X., Hobbs, R. P., & Coulombe, P. A. (2013). The expanding significance of keratin intermediate filaments in normal and diseased epithelia. Current Opinion in Cell Biology, 25(1), 47-56.

Peng, W., & Novak, N. (2015). Pathogenesis of atopic dermatitis. Clinical & Experimental Allergy, 45(3), 566-574.

Potts, R. O., & Francoeur, M. L. (1991). The influence of stratum corneum morphology on water permeability. Journal of Investigative Dermatology, 96(4), 495-499.

Proksch, E., Brandner, J. M., & Jensen, J. (2008). The skin: An indispensable barrier. Experimental Dermatology, 17(12), 1063-1072.

Proksch, E., Fölster-Holst, R., & Jensen, J. (2006). Skin barrier function, epidermal proliferation and differentiation in eczema. Journal of Dermatological Science, 43(3), 159-169.

Pummi, K., Malminen, M., Aho, H., Karvonen, S., Peltonen, J., & Peltonen, S. (2001). Epidermal tight junctions: ZO-1 and occludin are expressed in mature, developing, and affected skin and in vitro differentiating keratinocytes. Journal of Investigative Dermatology, 117(5), 1050-1058.

Quigley, D. A., Kandyba, E., Huang, P., Halliwill, K. D., Sjölund, J., Pelorosso, F., . . . Delrosario, R. (2016). Gene expression architecture of mouse dorsal and tail skin reveals functional differences in inflammation and cancer. Cell Reports, 16(4), 1153-1165.

Rinn, J. L., Wang, J. K., Liu, H., Montgomery, K., Van De Rijn, M., & Chang, H. Y. (2008). A systems biology approach to anatomic diversity of skin. Journal of Investigative Dermatology, 128(4), 776-782.

Roth, W., Kumar, V., Beer, H. D., Richter, M., Wohlenberg, C., Reuter, U., . . . Magin, T. M. (2012). Keratin 1 maintains skin integrity and participates in an inflammatory network in skin through interleukin-18. Journal of Cell Science, 125(Pt 22), 5269-5279. doi:10.1242/jcs.116574 [doi]

Ruether, A., Stoll, M., Schwarz, T., Schreiber, S., & Fölster‐Holst, R. (2006). Filaggrin loss‐of‐function variant contributes to atopic dermatitis risk in the population of northern germany. British Journal of Dermatology, 155(5), 1093-1094.

Sandilands, A., Sutherland, C., Irvine, A. D., & McLean, W. H. (2009). Filaggrin in the frontline: Role in skin barrier function and disease. Journal of Cell Science, 122(Pt 9), 1285-1294. doi:10.1242/jcs.033969 [doi]

Schweizer, J., Bowden, P. E., Coulombe, P. A., Langbein, L., Lane, E. B., Magin, T. M., . . . Wright, M. W. (2006). New consensus nomenclature for mammalian keratins. The Journal of Cell Biology, 174(2), 169-174. doi:jcb.200603161 [pii]

Scott, I. R., & Harding, C. R. (1986). Filaggrin breakdown to water binding compounds during development of the rat stratum corneum is controlled by the water activity of the environment. Developmental Biology, 115(1), 84-92.

Sevilla, L. M., Nachat, R., Groot, K. R., Klement, J. F., Uitto, J., Djian, P., . . . Watt, F. M. (2007). Mice deficient in involucrin, envoplakin, and periplakin have a defective epidermal barrier. The Journal of Cell Biology, 179(7), 1599-1612. doi:10.1083/jcb.200706187 [doi]

Smith, F. J., Irvine, A. D., Terron-Kwiatkowski, A., Sandilands, A., Campbell, L. E., Zhao, Y., . . . Lewis-Jones, S. (2006). Loss-of-function mutations in the gene encoding filaggrin cause ichthyosis vulgaris. Nature Genetics, 38(3), 337-342.

Steinert, P. M., & Parry, D. A. (1993). The conserved H1 domain of the type II keratin 1 chain plays an essential role in the alignment of nearest neighbor molecules in mouse and human keratin 1/keratin 10 intermediate filaments at the two- to four-molecule level of structure. The Journal of Biological Chemistry, 268(4), 2878-2887.

Sun, T. T., & Green, H. (1978). Keratin filaments of cultured human epidermal cells. formation of intermolecular disulfide bonds during terminal differentiation. The Journal of Biological Chemistry, 253(6), 2053-2060.

Tunggal, J. A., Helfrich, I., Schmitz, A., Schwarz, H., Gunzel, D., Fromm, M., . . . Niessen, C. M. (2005). E-cadherin is essential for in vivo epidermal barrier function by regulating tight junctions. The EMBO Journal, 24(6), 1146-1156. doi:7600605 [pii]

Van Smeden, J., Janssens, M., Gooris, G., & Bouwstra, J. (2014). The important role of stratum corneum lipids for the cutaneous barrier function. Biochimica Et Biophysica Acta (BBA)-Molecular and Cell Biology of Lipids, 1841(3), 295-313.

Weinstein, G. D., & van Scott, E. J. (1965). Autoradiographic analysis of turnover times of normal and psoriatic epidermis** from the dermatology branch, national cancer institute, national institutes of health, bethesda, maryland. public health

service, US department of health, education and welfare. Journal of Investigative Dermatology, 45(4), 257-262.

Wertz, P. W. (2005). Biochemistry of human stratum corneum lipids. Skin barrier (pp. 33-42) CRC Press.

Williams, M. L., & Elias, P. M. (1981). Stratum corneum lipids in disorders of cornification: Increased cholesterol sulfate content of stratum corneum in recessive x-linked ichthyosis. The Journal of Clinical Investigation, 68(6), 1404-1410.

Zhang, M., Li, B., Wu, S., Tan, J., Yang, Y., Marini, A., . . . Schikowski, T. (2017). A genome-wide association study of basal transepidermal water loss finds that variants at 9q34. 3 are associated with skin barrier function. Journal of Investigative Dermatology, 137(4), 979-982.

Zhang, H., Pasolli, H. A., & Fuchs, E. (2011). Yes-associated protein (YAP) transcriptional coactivator functions in balancing growth and differentiation in skin. Proceedings of the National Academy of Sciences of the United States of America, 108(6), 2270-2275. doi:10.1073/pnas.1019603108 [doi]

Curriculum Vitae

Krystynne Aguirre Leacock
DOB: 12/21/1988
Location of Birth: Washington D.C.
Current Address: 2313 Maryland Ave., Baltimore, MD 21218
Current Phone: 304.237.1649
E-mail Address: kleacoc1@jhu.edu

Research Interests

Current research interests include biochemical signaling pathways involved in carcinogenesis and skin disease. My principal aims include making a contribution that improves public health, educating others, and practicing medicine.

Work, Volunteer, and Research Experience

Graduate Researcher, Johns Hopkins University Bloomberg School of Public Health 2016-Current. Baltimore, MD

Graduate researcher in the Department of Biochemistry and Molecular Biology under the supervision of Dr. Pierre Coulombe, investigating intermediate filaments and skin barrier function using a CRISPR-Cas9 generated Keratin-14 C373A mouse model to examine the effect of disulfide bonding and skin barrier defects in the SC using *M.muluscus* as the model organism. Investigation required western blot analysis, genotyping, frozen tissue immunohistochemistry and paraffin embedding, IF staining, confocal microscopy, protein extraction, acrylamide gel electrophoresis, dermal and epidermal extractions, trans-epidermal water-loss measurements, and mouse colony management.

Medical Assistant, MOHS surgical Unit, Mountain State Medical Specialties 2012-2015. Morgantown, WV

Worked as a Medical Assistant during excisions, repairs, and biopsies of carcinomas and malignant melanoma, and atypical nevi. Responsibilities included: communicating pathology, recording patient histories on EMR, providing wound care, preparing examinations rooms for surgical procedures, biopsies and follow-up examinations. Interacted with patients, pharmacies, pharmaceutical companies/representatives, and insurance companies. Personally created and implemented surgical checklists at MSMS to ensure standardization of patient care. Provided patient care as a team member, established meaningful relationships with clients to ensure loyalty and promote positive & individualized patient care. I became CPR/AED Professional Rescuer/Health Provider certified. In addition, I was able to procure supplemental health benefits for over 500 underinsured employees.

Feldman E.N.T. Medical Assistant 2011. Chevy Chase, MD

Worked as a medical assistant in a multi-facility otolaryngology practice to ensure optimal patient care during routine and emergency office visits, by performing administrative and clinical duties: patient histories and vitals on chart or electronic medical records. I prepared examination rooms and assisted during examinations and procedures. I ensured the sanitation and maintenance of exam rooms and equipment and handled specimens, confidential records, and time-sensitive materials. Scheduled appointments and responded to patient requests.

Independent Student Research, Developmental Genetics, WVU Biology Department 2010-2011. Morgantown, WV

Investigated the effect of CK2 on the structure and function of chromatin using *D.melanogaster* and a PEV reporter gene. Investigated the evolutionary conservation of CK2's recognition sequence on potential targets across *M.muluscus* and *H.sapiens.* Worked independently to compile, analyze, and present results. Maintained and manipulated *D.melanogaste*r stock, measured experimental variables, and analyzed consensus sequences using *ClustalW.* Routinely sterilized equipment and reagents according to established protocols.

Capstone Research, WVU Biology Department 2010-2011. Morgantown, WV

Investigated environmental effects of heavy metals and increased carbon dioxide on *Chlorella pyreniodosa*. Leader in project management while collaborating with a team of student researchers to generate and analyze data to present results. Duties included sterilization of equipment, reagent creation, microscopic observations, and routine measurement and care of algal growth.

Research Assistant, Population Genetics, WVU Biology Department 2008-2009. Morgantown, WV

Investigated the effects of environmental influences on *Populus trichocarpa* using hydroponic solutions at the WVU Greenhouse and WVU Agronomy farm. Assisted in the harvest for the procurement of data to measure research variables using PCR, gel electrophoresis, DNA extraction and purification. Worked with a research team in the genomics facility to compile, analyze, and communicate experimental results.

Skills

Western Blot Analysis
Genotyping
Histologic Techniques
Microscopy
Investigation required western blot analysis, genotyping, tissue sectioning with OTC and paraffin embedding, Immuno-flourescence staining, confocal microscopy, protein extraction, acrylamide gel electrophoresis, dermal and epidermal extractions, trans-epidermal water-loss measurements, and mouse colony management.